

available at www.sciencedirect.com

ScienceDirect

www.elsevier.com/locate/molonc

Impact of selective anti-BMP9 treatment on tumor cells and tumor angiogenesis

Verena Brand^a, Christian Lehmann^a, Christian Umkehrer^a,
Stefan Bissinger^a, Martina Thier^b, Mariana de Wouters^b, Romi Raemisch^a,
Ute Jucknischke^a, Alexander Haas^c, Sebastian Breuer^c, Fabian Birzele^b,
Tomas Racek^b, Marco Reis^a, Erica Lorenzon^a, Frank Herting^a,
Michael Stürzl^d, Stefan Lorenz^c, Yvonne Kienast^{a,*}

^aDiscovery Oncology, Roche Pharmaceutical Research and Early Development (pRED), Roche Innovation Center, Munich, Germany

^bPharmaceutical Sciences, pRED, Roche Innovation Center, Basel, Switzerland

^cLarge Molecule Research, pRED, Roche Innovation Center, Munich, Germany

^dDivision of Molecular and Experimental Surgery, Department of Surgery, Universitätsklinikum Erlangen, Friedrich Alexander University Erlangen, Nürnberg, Germany

ARTICLE INFO

Article history:

Received 8 April 2016

Received in revised form

4 October 2016

Accepted 11 October 2016

Available online 20 October 2016

Keywords:

BMP9

ALK1

Angiogenesis

Pericytes

RCC

ET-1

ABSTRACT

The role of bone morphogenic protein 9 (BMP9) signaling in angiogenesis has been controversial, with a number of studies showing that it acts either as a pro-angiogenic or, conversely, as an anti-angiogenic factor in a context-dependent manner. Notably, BMP9 was also reported to function in both pro- or anti-tumorigenic roles during tumor progression. It has therefore remained unclear, whether selective BMP9 inhibition is a useful target for antibody therapy of cancer. To shed light on these questions, we characterized BMP9 expression in plasma of patients with different cancer indications and found elevated levels of pro-domains and precursor BMP9 with a strong response in renal cell carcinoma (RCC). These studies prompted us to evaluate the potential of selective anti-BMP9 cancer therapy in RCC. We generated a novel monoclonal therapeutic antibody candidate, mAb BMP9-0093, that selectively targets all different BMP9 variants but does not bind to the closest homolog BMP10. *In vitro*, mAb BMP9-0093 treatment inhibited signaling, endothelin-1 (ET-1) production and spreading of endothelial cells and restored BMP9-induced decrease in pericyte migration and attachment. Furthermore, BMP9-mediated epithelial–mesenchymal transition of renal cell carcinoma cells was reversed by mAb BMP9-0093 treatment *in vitro*. *In vivo*, mAb BMP9-0093 showed significant anti-tumor activity that was associated with an increase in apoptosis as well as a decrease in tumor cell proliferation and ET-1 release. Furthermore, mAb BMP9-0093 induced mural cell coverage of endothelial cells, which was corroborated by a reduction in vascular permeability, demonstrated by a diminished penetration of omalizumab-Alexa 647 into

Abbreviations: HHT, hereditary hemorrhagic telangiectasia; mAb, monoclonal antibody; ELISA, enzyme-linked immunosorbent assay; BMP, bone morphogenic protein; ET-1, endothelin-1; GDF, growth and differentiation factor; ALK1, activin receptor-like kinase 1; ENG, endoglin; HCC, hepatocellular carcinoma; RCC, renal cell carcinoma; EMT, epithelial to mesenchymal transition; SPR, surface plasmon resonance; HUVEC, human umbilical vein endothelial cell; hPC, primary human pericytes.

* Corresponding author. Fax: +49 8856 60 79 6308.

E-mail address: yvonne.kienast@roche.com (Y. Kienast).

<http://dx.doi.org/10.1016/j.molonc.2016.10.002>

1574-7891/© 2016 Federation of European Biochemical Societies. Published by Elsevier B.V. All rights reserved.

tumor tissue. Our findings provide new evidence for a better understanding of BMP9 contribution in tumor progression and angiogenesis that may result in the development of effective targeted therapeutic interventions.

© 2016 Federation of European Biochemical Societies. Published by Elsevier B.V. All rights reserved.

1. Introduction

Bone morphogenetic proteins (BMP2–BMP15) are potent growth factors that belong to the transforming growth factor- β (TGF- β) superfamily. BMP9, also known as growth and differentiation factor 2 (GDF2), is a secreted, dimeric cytokine with pleiotropic functions under physiological and pathological conditions. BMP9 is described as a hematopoietic, hepatogenic, osteogenic, and chondrogenic factor that is also involved in neuronal differentiation, glucose homeostasis, tumor progression, and angiogenesis (Lopez-Coviella et al., 2000; Chen et al., 2003; David et al., 2008; Luther et al., 2011; Herrera et al., 2014). The complexity of BMP9 function is further increased by the existence of three known alternative variants, circulating in plasma (i) as an unprocessed inactive form that can be further activated by furin cleavage (BMP9 precursor protein), (ii) an active form composed of the mature form non-covalently associated with two pro-domains (BMP9•pro-domain), and (iii) as an active mature ligand dimer without pro-domains (mature BMP9) (Brown et al., 2005; Bidart et al., 2012; Kienast et al., 2016).

Activin receptor-like kinase 1 (ALK1) is a specific type I receptor for BMP9 that is expressed on both blood and lymphatic endothelial cells (Cunha and Pietras, 2011). In addition to its expression in the endothelium, ALK1 has been reported in chondrocytes (Finsson et al., 2008), cardiomyocytes (Su et al., 2004), monocytes (Sanz-Rodriguez et al., 2004), neural crest stem cells (Mancini et al., 2007), skin fibroblasts (Beger et al., 2006), microglia (Konig et al., 2005) and myoblasts (Velasco et al., 2008). While BMP9 has recently been highlighted by the characterization of its binding to ALK1, the observed effects mediated by BMP9 are both pro- and anti-angiogenic and seem to depend on the context, and still need to be further elucidated (David et al., 2008; Cunha et al., 2010; Larrivee et al., 2012). The vascular effects of BMP9 in cancer-related angiogenesis are largely unknown. Moreover, BMP9 was shown to function in both pro- or anti-tumorigenic roles during tumor progression (Herrera et al., 2009; Wang et al., 2011).

ALK1 and its co-receptor endoglin (ENG) have been identified as causal genes for the genetic vascular disorder known as hereditary hemorrhagic telangiectasia (HHT) (McAllister et al., 1994; Johnson et al., 1996). Interestingly, mutations in BMP9 have been identified in individuals with a vascular disorder phenotypically overlapping with HHT (Wooderchak-Donahue et al., 2013). $Alk1^{+/-}$ and $Eng^{+/-}$ mice exhibit abnormal vascular phenotypes reminiscent of those of HHT patients, while $Alk1^{-/-}$ and $Eng^{-/-}$ mice die at E11 because of major angiogenesis defects (Bourdeau et al., 2000; Srinivasan et al., 2003). BMP9-knockout neonates

and adult mice show an abnormal lymphatic vasculature and a decrease in draining efficiency (Levet et al., 2013), while other vascular functions of BMP9 during embryogenesis and development are compensated by BMP10, the closest homolog for BMP9 sharing 65% similarity at the protein level (Ricard et al., 2012; Chen et al., 2013). This data suggest that BMP9 and BMP10 are redundant for vascular development, while BMP9 is critical for lymphatic development.

The roles of BMP9 in embryonic vascular development and adult angiogenesis remain controversial. On the one hand, it was reported that BMP9 induces proliferation and migration of endothelial cells by triggering the expression of VEGFR2 and TIE-2, both of which stimulate blood endothelial cell proliferation (Suzuki et al., 2010). By contrast, recent studies have implicated BMP9 signaling in the maintenance of a quiescent endothelial stalk cell fate and as a negative regulator of retinal angiogenesis (Ricard et al., 2012; Larrivee et al., 2012). In this respect, ALK1 signaling is shown to synergize with Notch signaling in stalk cells to induce expression of the Notch targets HEY1 and HEY2, thereby repressing tip cell formation and angiogenic sprouting (Larrivee et al., 2012). Furthermore, BMP9-induced signaling through ALK1 results in inhibition of both VEGF- and FGF-induced angiogenesis *in vitro* (Scharpfenecker et al., 2007; David et al., 2007), concluding that BMP9 is an anti-angiogenic factor, and that BMP9 interacts with ALK1 to promote endothelial cell quiescence and vessel maturation (Lamouille et al., 2002). The mechanisms underlying the proposed BMP9-mediated vessel maturation are however not fully understood, and it remains unclear, how BMP9 affects signaling between endothelial cells and the neighboring mural cells.

While BMP9 is normally expressed in the liver, expression of BMP9 in tumors has been reported previously (Herrera et al., 2009; Wang et al., 2016). In ovarian tumors, BMP9 expression is shown to be elevated and to promote tumor cell proliferation by an autocrine mechanism (Herrera et al., 2009). In hepatocellular carcinoma (HCC), BMP9 is described as survival (Herrera et al., 2013) and epithelial to mesenchymal transition (EMT) inducing factor (Li et al., 2013). By contrast, BMP9 expression is reportedly decreased or absent in prostate cancer and forced overexpression mediates apoptosis (Ye et al., 2008). Furthermore, exogenous BMP9 is shown to inhibit proliferation and metastasis of breast cancer cells (Wang et al., 2011) and to induce apoptosis in myeloma cells (Olsen et al., 2014). The role of BMP9 in renal cell carcinoma (RCC), a particularly angiogenic cancer type, is unclear. BMP9 can stimulate endothelial cell-mediated release of endothelin-1 (ET-1) (Star et al., 2010), a potent vasoconstrictor that has been shown to play an important role in both normal and diseased kidney

(Pflug et al., 2007). These data suggest a possible hint towards a relationship between BMP9 signaling and RCC, that warrants further investigation.

Monoclonal antibody approaches targeting the receptors ALK1 (PF-03446962) and ENG (TRC105), as well as ALK1-Fc (dalantercept, previously known as ACE-041), a ligand trap targeting BMP9 and BMP10, have been described as inhibitors of angiogenesis and tumor growth in mouse models (Takahashi et al., 2001; Cunha et al., 2010; Hu-Lowe et al., 2011). This led to a multicenter randomized phase II study that is currently underway exploring the combination of dalantercept plus axitinib versus axitinib plus placebo in patients with advanced RCC refractory to anti-VEGF therapy (Wang et al., 2016). Furthermore, selective expression of BMP9 in tumors increases blood vessel density, suggesting BMP9 to function as an inducer of tumor angiogenesis (Yoshimatsu et al., 2013). Interestingly, it was recently reported that cancer patients with HHT have improved survival outcomes (Duarte et al., 2014).

Thus, although BMP9 has been implicated in angiogenesis during development and disease, its functions remain controversial and context-specific. To date, nobody has addressed the effect of selective pharmacological targeting of BMP9 on tumor progression and angiogenesis *in vivo*. Elevated plasma levels of pro-domains and precursor BMP9 in cancer patients, particularly in RCC, prompted us to investigate the mode of action of a novel monoclonal therapeutic antibody candidate, mAb BMP9-0093 that neutralizes all circulating BMP9 variants but does not bind to BMP10. Anti-BMP9 mAb BMP9-0093 interfered with BMP9-induced effects on RCC tumor cells, endothelial cells and pericytes *in vitro*. Notably, using distinct migration assays, we detected a BMP9-induced decrease in pericyte migration and attachment to endothelial cells that was reversed by mAb BMP9 0093 treatment. In addition, BMP9 blockade delayed tumor growth of A-498 RCC xenografts *in vivo*, and resulted in an increase in mural cell coverage of tumor vessels, associated with a reduction in vascular permeability. Our results provide mechanistic insights into the role of BMP9 in tumor progression and angiogenesis and encourage further investigation of BMP9 targeting agents in cancer therapy.

2. Materials and methods

2.1. Generation of anti-BMP9 mAb BMP9-0093 and recombinant BMP9 proteins

Anti-BMP9 mAb BMP9-0093 was generated at Roche Innovation Center Munich by hamster immunization with full-length recombinant human BMP9 and subsequent cloning into a mouse IgG2a backbone. Cloning, expression and purification of BMP9 precursor protein, BMP9•pro-domain complex and mature BMP9 cytokine was performed as described previously (Kienast et al., 2016). Based on a dose–response experiment (Figure S1), BMP9 was used at a concentration of 50 ng/ml in the majority of the experiments (details below). Other recombinant human proteins used for *in vitro* assays were purchased from R&D Systems.

2.2. Blood donors

Plasma samples (total 302, 285 cancer cases of 12 different cancer types and 17 healthy controls) were purchased from Indivumed (Hamburg, Germany). Histopathological diagnoses were confirmed after surgical resection of the tumors. None of the patients had received any treatment prior to surgery. The control plasma samples were collected from healthy individuals with no history of malignant diseases and no inflammatory conditions using the same collection and sampling procedures. All cases and controls were of Western European descent. Written informed consent was obtained from all individuals permitting the commercial use of donated blood samples. The study was approved by the Data Protection Authority Hamburg. Procedures in place respect the German data protection laws as well as US regulations. Indivumed acts in strict compliance with The Declaration of Helsinki and The Convention on Human Rights and Biomedicine. The ELISA setup for the detection of circulating BMP9 variants in plasma of healthy and cancer patients was performed as previously described (Kienast et al., 2016).

2.3. BMP9 and BMP10 binding ELISA

For the BMP9 and BMP10 binding ELISA, 100 ng/ml BMP9 and BMP10 were coated overnight at 4 °C in PBS on Maxisorp 384-well plates (ThermoScientific). Plates were washed with PBST (PBS + 0.05% Tween 20) and blocked with 2% (w/v) BSA in PBST for 5–8 h at 20 °C. Blocking solutions were decanted, and anti-BMP9 mAb BMP9-0093 was applied at serial dilutions in PBST with 2% (w/v) BSA and incubated at 4 °C overnight. Plates were washed three times with PBST, followed by the addition of secondary IgG conjugated with HRP (Jackson) at 1:5000 in PBST + 1% BSA. After overnight incubation at 4 °C, plates were washed with PBST and color was developed with 3,3',5,5' tetramethylbenzidine. After stopping with 1 M H₂SO₄, plates were read at 450 nm.

2.4. Surface plasmon resonance (SPR)

All experiments were performed on Biacore T100 and T200 instruments in running buffer PBS containing 0.05% (v/v) Tween 20. Dilution buffer consisted of running buffer supplemented with 1 mg/ml BSA. Standard amine coupling was carried out as recommended by the supplier GE Healthcare. Binding signals were double referenced against blank buffer and a reference cell containing amine coupled anti-mouse Fc antibody only. Kinetic constants were calculated from fitting to a 1:1 Langmuir binding model (RI = 0). Listed K_D represents avidity instead of affinity due to possible bivalent binding of dimeric BMP9 to mAb BMP9-0093. Anti-BMP9 mAb BMP9-0093 was captured via anti-mouse Fc (GE Healthcare). Series with increasing concentrations of BMP9-variants were injected with an association phase of 180 s followed by a dissociation phase of 300–3600 s. Interaction partners were analyzed in duplicates on a CM5 sensor chip at 37 °C at a flow rate of 50 µl/min. Capture levels were adjusted to achieve a maximal analyte response R_{max} of 30–40 RU. Mature BMP9 and BMP9•pro-domain complex were analyzed in concentrations of c = 0.14–11.1 nM, human precursor BMP9 was analyzed in

concentrations of $c = 18.5$ – 1500 nM. Capture antibody was amine coupled and regenerated as recommended by the vendor.

2.5. Cell lines and culture conditions

Low passage human umbilical vein endothelial cells (HUVEC, PromoCell) were cultured in enriched endothelial cell growth medium (ECGM, PromoCell) containing endothelial cell medium supplement (PromoCell) and 10% fetal calf serum (FCS; PAN Biotech). Human placental pericytes (hPC, PromoCell) were maintained in culture in pericyte growth medium (PGM, PromoCell) supplemented with 10% FCS. The hybrid human umbilical vein cell line, EA.hy926 (ATCC), was routinely cultured in RPMI1640 supplemented with 10% FCS and 2 mM L-glutamine (PAA Laboratories). EA.hy926 cells were established by fusing primary human umbilical vein cells with a thioguanine-resistant clone of A549. Electron photomicrographs demonstrate cytoplasmic distribution of Weibel–Palade bodies and tissue-specific organelles, characteristics of differentiated endothelial cell functions such as angiogenesis, homeostasis/thrombosis, blood pressure and inflammation (Edgell et al., 1983; Edgell et al., 1990). Human kidney carcinoma A-498 cells (ATCC) were grown in MEM Eagle (PAN Biotech) supplemented with 10% FCS and 2 mM L-glutamine. All cells were maintained at 37 °C in a water-saturated atmosphere at 5% CO₂. Cell lines were characterized by STR-PCR and routinely tested for mycoplasma, bacterial and fungal infection.

2.6. Endothelin-1 ELISA

Endothelin-1 production was detected according to manufacturer's instructions (Quantikine Endothelin-1, R&D Systems). For antibody characterization, 4×10^4 EA.hy926 cells per well were seeded in 50 µl RPMI1640 (0.5% FCS) in 96-well plates and incubated for 24 h. Antibodies (MAB3209 (R&D Systems), Isotype Control Mouse IgG2b (BioLegend) and mAb BMP9-0093) were pre-incubated with BMP9 (10 ng/ml) in tubes for 15 min at 37 °C to allow for antibody binding and were then added to the cells and incubated for 50 h. The cell culture supernatant was then used for the detection of ET-1 by ELISA. The absorbance was read at a wavelength of 450 nm with a correction set at 570 nm. The same ELISA was used for the detection of ET-1 in tumor lysates and cell culture supernatants of HUVEC. Five tumors per group were lysed in 10 µl/mg tumor lysis buffer (10 mM Tris, 137 mM NaCl, 1% Triton, 10% Glycerin, pH 8.0) supplemented with Halt™ Protease Inhibitor Cocktail (Thermo Scientific™). 2×10^3 HUVEC per well were seeded in 50 µl ECGM (2% FCS) in 96-well plates and allowed to attach before stimulation w/and w/o BMP9 (10 ng/ml or 50 ng/ml) in ECGM (2% FCS) for 72 h.

2.7. Functional electronic cell sensor assay (xCELLigence)

EA.hy926 cells were pre-incubated with BMP9 (5 ng/ml) ± mAb BMP9-0093, MAB3209 and Isotype Control Mouse IgG2b. Ninety six-well plates were coated with collagen (Roche) dissolved in sterile PBS (2 mg/ml) for 1 h at 37 °C. Background

signal of plates was measured in the presence of 100 µl cell culture medium (RPMI1640, 5% FCS). To start measurement, 100 µl cell suspension (1.5×10^4 cells per well in triplicates) were transferred to a 96-well plate (E-plate) connected to a real-time cell electronic sensing device (xCELLigence System/Real Time Cell Analyzer MP Instrument, Roche). Real-time cellular morphogenic and phenotypical changes (attachment, filopodia formation, spreading and proliferation) over a 30 h time frame were monitored and recorded; the readout (changes in impedance) at $t = 15$ h was displayed as an arbitrary unit called Cell Index.

2.8. Wound closure assay

3.5×10^4 HUVEC or 2.1×10^4 hPC per well were seeded in the respective growth medium supplemented with 10% FCS in culture-inserts 2 well (ibidi, 81176) and grown to confluence. Cells were starved overnight prior to stimulation in endothelial cell basal medium (ECBM, PromoCell) supplemented with 2% FCS. After removal of inserts, cells were stimulated with either BMP9 (50 ng/ml), PDGF-BB (40 ng/ml), or bFGF (30 ng/ml) in serum-reduced medium containing 2% FCS. Anti-BMP9 mAb BMP9-0093 (10 µg/ml) was pre-incubated with BMP9 (50 ng/ml) for 60 min at 37 °C to allow antibody binding. In a preliminary experiment gaps were imaged up to 24 h using Leica DM IL LED microscope to determine time points, when positive control was already closed and unstimulated control was almost closed. Ratio of gap closure at 0 and 12 h for HUVEC and 24 h for hPC is shown as percentage.

2.9. Pericyte-endothelial cell attachment assay

HUVEC and hPC were labeled with green fluorescent dye PKH67 and red fluorescent dye PKH26, respectively, according to the manufacturer's instructions (Sigma Aldrich). 3.5×10^4 HUVEC were seeded in one well of the culture-inserts 2 well (ibidi, 81176) in ECGM with 10% FCS. 2.1×10^4 hPC were seeded in the other well in PGM with 10% FCS. Cells were grown to confluence. After removing the inserts, medium was replaced with ECBM (w/o FCS) containing BMP9 (50 ng/ml) w/and w/o mAb BMP9-0093 (10 µg/ml). Cells were imaged after 48 h using Leica DM IL LED microscope. Amount of attached pericytes was determined as red fluorescent area located next to HUVEC (green) and quantified by automated analysis (Image Intensity Threshold Tool, Roche).

2.10. In vitro cell imaging

A-498 cells were treated with 100 ng/ml BMP9 in 96-well plates. After 72 h, cells were fixed with 4% (v/v) PFA in PBS, washed twice and incubated overnight in blocking buffer (Odyssey, LI-COR) containing detergent and staining antibodies anti-Vimentin A555 (Cell Signaling) and Hoechst 33258 (Invitrogen). Cells were then washed twice in PBS and fluorescence was measured on an Operetta high content screening system (PerkinElmer). Data were analyzed using Harmony software version 3.5.2 (PerkinElmer) and Excel.

2.11. Caspase-Glo® 3/7 assay

5×10^3 cells were seeded in a 96-well culture plate (BRAND) filled with growth medium including 10% FCS alone or supplemented with 100 ng/ml BMP9 and allowed to attach for 48 h. Cells were serum starved (w/o FCS) overnight (16 h) to induce caspase activity that was determined using the Caspase-Glo® 3/7 Assay (Promega).

2.12. Cell viability assay (CellTiter-Glo®)

5×10^3 cells (A-498) were seeded in a 96-well culture plate (BRAND) filled with growth medium supplemented with 10% FCS and allowed to attach. Cells were starved overnight prior to stimulation with BMP-9 (50 ng/ml or 100 ng/ml) or ET-1 (25 ng/ml or 250 ng/ml) in serum reduced medium (2% FCS) for 72 h. Cell viability was determined using the CellTiter-Glo® Luminescent Cell Viability Assay (Promega).

2.13. Immunoblotting

Cells were washed with ice cold PBS, lysed in lysis buffer (20 mM Tris-HCl pH 7.6, 150 mM NaCl, 10 mM NaF, 2 mM Na-orthovanadat, 0.5% Na-deoxycholate, 0.1% SDS, 1.0% NP-40, and protease-inhibitor cocktail, consisting of phosStop and complete-mini tablets; Roche) and incubated for 20 min on ice. Protein concentration was determined using the BCA Protein Assay (Thermo Scientific) to ensure equal gel loading. Proteins were separated on a 10% SDS-PAGE gel under reducing conditions and proteins were transferred to nitrocellulose membranes using iBlot® technology (Novex™). After blocking in 4% skim milk for 1 h at room temperature (RT), blots were probed with specific antibodies to ALK1 (1:1000; Abcam, ab108207), ALK2 (1:1000; Cell Signaling, 4398), ALK5 (1:1000, Cell Signaling, 3712), ActRIIA (1:5000; Abcam, ab134082), ActRIIB (1:1000; Abcam, ab128544), BMPRII (1:1000; Cell Signaling, 6979), Smad 1 (1:1000; Cell Signaling, 9743), Smad 2/3 (1:1000; Cell Signaling, 3102), Phospho-Smad1 (Ser463/465)/Smad5 (Ser463/465)/Smad8 (Ser465/467) (1:1000; Cell Signaling, 9511), Phospho-Smad2 (Ser465/467)/Smad3 (Ser423/425) (1:1000; Cell Signaling, 8828), Vimentin (1:1000; Cell Signaling, 5741), N-Cadherin (1:1000; Cell Signaling, 13116), Claudin-1 (1:1000; Cell Signaling, 13255), β -Catenin (1:1000; Cell Signaling, 8480), Snail (1:1000; Cell Signaling, 3879), human E-Cadherin (1:1000; BD Bioscience, 610181), murine E-Cadherin (1:1000; Cell Signaling, 3195), murine Endoglin (1:1000; Abcam, ab21222) and human Endoglin (1:1000; BD Bioscience, 611315). Anti-human β -actin antibody (1:1000; Cell Signaling, 4970) served as loading control. Subsequently, the membranes were incubated for 1 h at RT with the appropriate horseradish peroxidase conjugated secondary anti-rabbit or anti-mouse antibodies (1:2000; Cell Signaling, 7074 and 7076). Bands were visualized by chemiluminescence using Super Signal® West Femto Maximum Sensitivity Substrate (Thermo Scientific).

2.14. Animal care and tumor establishment

8 to 10 week-old female SCID/beige (Charles River Laboratories) were maintained under specific pathogen-free

conditions with daily cycles of 12 h light/12 h darkness. All experimental procedures were conducted in accordance with committed guidelines as approved by local government (GV-Solas; Felasa; TierschG). For tumor establishment, $100 \mu\text{l}$ PBS containing 5×10^5 A-498 cells passage 3 were injected subcutaneously into the right flank of SCID/beige mice. Treatment of animals started at day of randomization, at a mean tumor volume of 100 mm^3 .

2.15. Histology, immunostaining and quantification

Tumor vessels were stained in $2.5 \mu\text{m}$ paraffin sections using a rat anti-mouse CD31 antibody (dianova) and a biotinylated rabbit anti-rat IgG antibody (Vector Labs). Number and size of vessels were quantified by automated analyses (Definiens) on entire slides (5 tumors per group) and microvessel density was calculated as vessels per mm^2 viable tissue. Rabbit anti-phospho-Histone H3 (Ser10) antibody (Millipore) and corresponding secondary goat anti-rabbit IgG antibody (Jackson) were used to stain proliferating cells on $2.5 \mu\text{m}$ paraffin sections. Signal was quantified by automated analysis as count of positive cells per mm^2 on entire slides (Image Intensity Threshold Tool, Roche; 5 tumors per group). Rabbit anti-cleaved Caspase-3 antibody (Cell Signaling) and corresponding secondary goat anti-rabbit IgG antibody (Jackson) were used to stain apoptotic areas on $2.5 \mu\text{m}$ paraffin sections. Signal was quantified by automated analysis as positive stained area per tumor area on entire slides (Image Intensity Threshold Tool; 5 tumors per group). In order to stain perfused tumor vessels, Alexa-750-labeled *Bandeiraea simplicifolia* lectin ($100 \mu\text{g}$) was injected intravenously 5 min prior to sacrifice. Blood vessels were stained against CD31 (Pharmingen) on $10 \mu\text{m}$ cryo sections. Perivascular cells were detected on $2 \mu\text{m}$ paraffin sections with specific antibodies to Desmin (Abcam) or α -SMA (Sigma Aldrich) or on $10 \mu\text{m}$ cryo sections with anti-NG2 antibody (Millipore). Corresponding secondary antibodies included goat anti-rabbit IgG (Jackson), goat anti-rat IgG (Jackson) and goat anti-rabbit IgG (Invitrogen). Vessel coverage was calculated by automated analysis (Vessel/pericyte Analysis Tool, Roche) as the percentage of either α -SMA, NG2 or desmin positive vessels compared with the number of lectin positive vessels. The average signal for each slide (based on five random areas of $2000 \times 1000 \mu\text{m}$) is plotted (5 tumors per group).

2.16. Ultramicroscopy

To visualize and quantify tumor vessel architecture and penetration capability of therapeutic antibodies into tumor tissue, five tumor-bearing mice per treatment group were injected i.v. with omalizumab-Alexa 647 ($50 \mu\text{g}$) 24 h and lectin-Alexa 750 ($100 \mu\text{g}$) 5 min prior sacrifice. Tumors were cleared as previously described (Dodt et al., 2007) to avoid tissue scattering and light absorption and to provide optical transparency. The cleared specimens were scanned with a commercial ultramicroscope (LaVision BioTec, Bielefeld, Germany). Vessel quantification and antibody penetration analyses were performed as previously described (Dobosz et al., 2014).

2.17. Statistical analysis

Results are expressed as mean \pm SEM. All experiments were performed at least twice. Differences between experimental groups were analyzed using an unpaired, two-tailed Student t test or Wilcoxon signed-rank test, respectively. A value of $p = 0.05$ was considered as statistically significant.

3. Results

3.1. Pro-domain complexed BMP9 levels are elevated in plasma of cancer patients

BMP9 is synthesized as a large inactive precursor consisting of an N-terminal signal peptide directing secretion, a pro-domain, and a C-terminal mature peptide. Enzymatic processing by pro-protein convertases (e.g., furin) generates two active cytokines, mature BMP9 and BMP9•pro-domain (consisting of the mature BMP9 dimer and two non-covalently associated pro-domains; Figure S2). As part of a systematic effort to characterize all different circulating BMP9 variants in biological samples, we previously reported a three steps ELISA approach (Kienast et al., 2016). Briefly, our recent data revealed displacement of pro-domains from the BMP9•pro-domain complex after antibody (and also BMP9 receptor) binding (Kienast et al., 2016). As a consequence, three different ELISAs were developed: (i) “mature BMP9 ELISA” detecting (a) mature BMP9 and (b) antibody-displaced mature BMP9 domain originating from BMP9•pro-domain complex

(Figure S3A); (ii) “precursor BMP9 ELISA” detecting precursor BMP9 protein (Figure S3B); and (iii) “pro-domain ELISA” detecting (a) unbound pro-domains and (b) antibody-displaced pro-domains originating from BMP9•pro-domain complex (Figure S3C). Additionally, this assay detects also precursor BMP9 (Figure S3C). To quantify the amount of pro-domains present in the sample, the result of the “precursor BMP9 ELISA” and the “pro-domain ELISA” were subtracted. In the current study, BMP9 was measured in plasma of cancer patients with different tumor entities ($n = 285$ in total; table S1). The results of the three above mentioned ELISAs revealed a precursor BMP9 proportion of 28% in cancer patient plasma. The proportion of BMP9 that was measured with the “mature BMP9 ELISA” (0.2%) was composed of (a) mature BMP9 and (b) BMP9•pro-domain. The proportion of BMP9 that was measured with the “pro-domain ELISA” (71.8%) was composed of (a) unbound pro-domains and (b) BMP9•pro-domain. Considering the double signal measured for BMP9•pro-domain complex in both “mature BMP9” and “pro-domain” ELISA assays, we estimated that the majority of BMP9 (~71%) in the biological samples were pro-domain fragments (Figure 1A). BMP9 concentration in the plasma of cancer patients grouped by different tumor entities (Table S1) was furthermore compared with healthy individuals (Figure S4). Significant differences were observed in the levels of RCC patients (Figure 1B–D; $n = 15$ RCC cases and 17 healthy controls). Here, mean mature BMP9 concentration levels (58.5 pg/ml, range 19.2–287.3) were significantly lower in RCC patients ($p < 0.001$) than in healthy controls (92.2 pg/ml, range 65.5–128.5; Figure 1B). In contrast, average concentrations

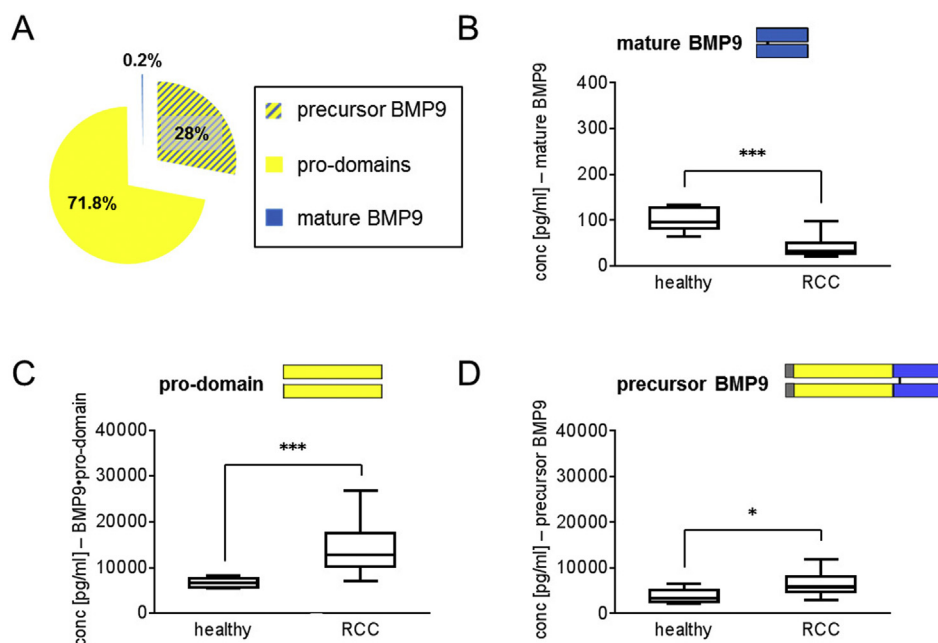


Figure 1 – Precursor BMP9 and pro-domain levels are elevated in plasma of cancer patients. (A) Pie chart representing the percentage of mature BMP9, precursor BMP9, and pro-domains circulating in human plasma of cancer patients ($n = 285$). A previously reported ELISA assay setup (Kienast et al., 2016) reveals reduced levels of (B) mature BMP9 ($***p \leq 0.001$ versus control), and elevated levels of (C) pro-domains ($***p \leq 0.001$ versus control), and (D) precursor BMP9 ($*p \leq 0.05$ versus control) in plasma of RCC patients ($n = 15$ RCC cases and 17 healthy controls).

of pro-domains (15.7 ng/ml, range 7.0–35.5; $p < 0.001$) and precursor BMP9 (6.5 ng/ml, range 3.0–11.9; $p < 0.05$) were significantly higher in RCC patients than in healthy controls (6.8 ng/ml, range 5.5–8.2 and 3.8 ng/ml, range 2.2–6.5; Figure 1C and D). An influence of BMP9 levels on overall survival or progression-free survival was not investigated.

3.2. Characterization of anti-BMP9 mAb BMP9-0093

Elevated plasma levels of pro-domain complexed BMP9 in RCC patients prompted us to generate a novel BMP9-selective monoclonal antibody to investigate selective anti-BMP9 therapy in tumor bearing mice. Anti-BMP9 mAb BMP9-0093 was generated by hamster immunization with full-length recombinant human BMP9 at the Roche Innovation Center Munich. The heavy and light chain variable regions were subcloned into mouse IgG2a and kappa constant domains, respectively. The resulting recombinant chimeric mAb BMP9-0093 binds to recombinant human, cynomolgus monkey, and mouse BMP9 but does not bind to BMP10 (Figure 2A). Furthermore, binding kinetics to circulating BMP9 variants were investigated. SPR analysis revealed that mAb BMP9-0093 binds potently to human mature BMP9 and BMP9•pro-domain with high avidity and an apparent K_D in the low pM range (Figure 2B and C, Table 1); precursor BMP9 was bound with an apparent K_D in the low nM range (Figure 2D). To characterize mAb BMP9-0093 in functional cell-based assays, we measured endothelin-1 secreted by immortalized endothelial EA.hy926 cells in response to BMP9 stimulation. Figure 3A shows the respective ELISA using the commercially available anti-BMP9 antibody MAB3209 as a reference. Both antibodies inhibited BMP9-induced endothelin-1 expression (Figure 3A, $p < 0.05$). The established assay was then used to evaluate the IC_{50} of mAb BMP9-0093 which potently and dose-dependently inhibited BMP9-induced endothelin-1 production of EA.hy926 cells (Figure 3B; $IC_{50} = 1.1$ ng/ml). Using an electronic cell sensor high throughput screening (HTS) assay (xCELLigence) in which cellular phenotypical changes were measured in real time, we observed that MAB3209 and BMP9-0093 rapidly inhibited BMP9-induced decrease in EA.hy926 morphologic changes (Figure 3C), with an IC_{50} for mAb BMP9-0093 of 0.5 ng/ml (Figure 3D). The neutralizing activity and potency of mAb BMP9-0093 (10 μ g/ml) was further confirmed by its ability to inhibit BMP9 (50 ng/ml) induced Smad 1/5/8 and Smad 2/3 phosphorylation not only in EA.hy936 cells, but also in primary human endothelial cells (HUVEC). Furthermore, we observed BMP9-mediated Smad 1/5/8 but not Smad 2/3 phosphorylation in primary human pericytes (hPC), which could also be abrogated by treatment with mAb BMP9-0093 (Figure 3E). Expression of relevant BMP9 receptors ALK1, BMPRII, ActRIIA and ActRIIB on HUVEC and hPC was confirmed on mRNA level (Figure S5A). Data were corroborated on protein level by Western blot analyses, which additionally revealed the expression of the type I receptors ALK2, ALK5 and the co-receptor ENG (Figure S5B). In addition, western blot analysis confirmed expression of receptors ALK1, ALK2, ALK5, BMPRII, ActRIIA, ActRIIB and ENG on EA.hy926 cells (Figure S5B).

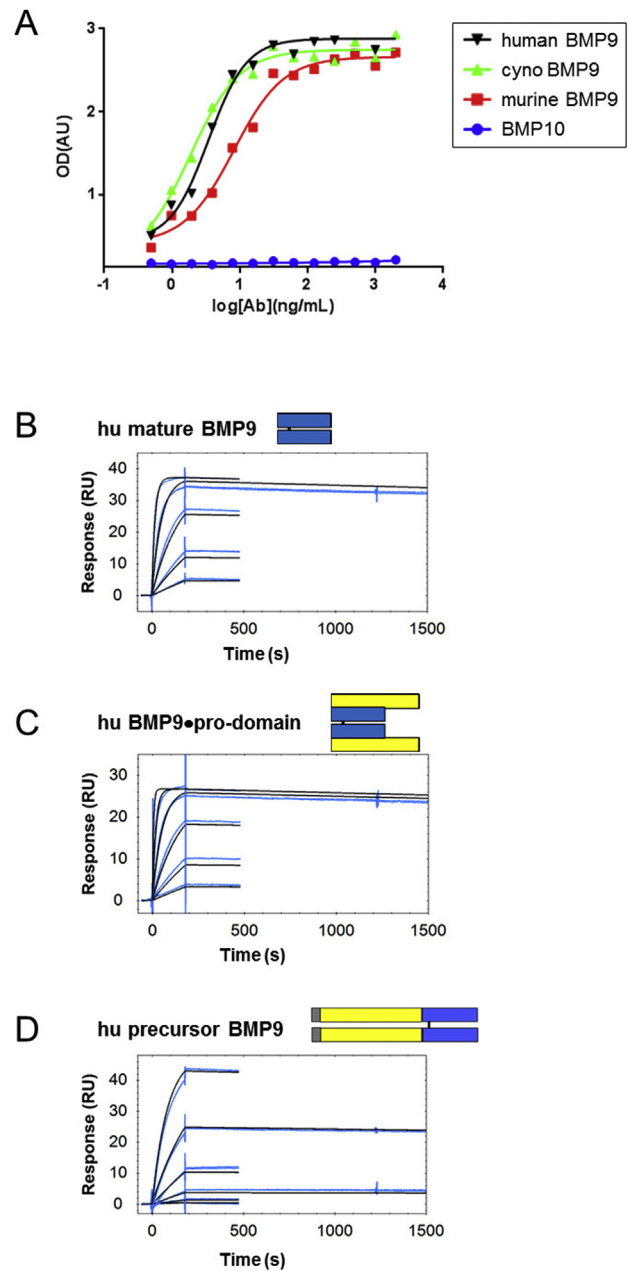


Figure 2 – Target binding characteristics of anti-BMP9 mAb BMP9-0093. (A) Anti-BMP9 mAb recognizes cynomolgus, murine and human BMP9 mature cytokine, but does not bind to BMP10 as demonstrated by ELISA. (B–D) SPR sensorgrams of BMP9 variants binding to captured anti-BMP9 mAb BMP9-0093 on a CM5 sensor chip. Kinetic profiles at 37 °C of (B) human mature BMP9, (C) human BMP9•pro-domain complex, and (D) human precursor BMP9 were measured in concentration series with duplicates of each concentration (shown in blue), evaluated with a regular 1:1 Langmuir binding model (shown in black).

3.3. Anti-BMP9 mAb BMP9-0093 restores BMP9-induced decrease in pericyte migration and attachment

BMP9-induced Smad 1/5/8 phosphorylation in hPC (Figure 3E) prompted us to investigate further effects of BMP9 signaling

Table 1 – Binding parameters for BMP9 variants binding to mAb BMP9-0093 at 37 °C.

On chip	BMP9 variant in solution	k_a	k_d	$t_{1/2}$	K_D
		$[M^{-1} s^{-1}]$	$[s^{-1}]$	$[min]$	$[M]$
mAb BMP9-0093	hu mature BMP9	$6.8 \times 10^6 \pm 0.2\%$	$<5.0 \times 10^{-5} \pm 0.6\%$	>231.0	$<7.4 \times 10^{-12}$
	hu BMP9•pro-domain	$6.4 \times 10^6 \pm 0.3\%$	$<5.0 \times 10^{-5} \pm 1.0\%$	>231.0	$<7.9 \times 10^{-12}$
	hu precursor BMP9	$7.9 \times 10^3 \pm 0.1\%$	$<5.0 \times 10^{-5} \pm 0.6\%$	>231.0	$<6.3 \times 10^{-9}$

Association (k_a) and dissociation (k_d) rate constants, half times ($t_{1/2}$) and resulting dissociation equilibrium constants K_D determined from the fits are listed with the standard errors. Langmuir 1:1 Model (RI = 0) was used. Listed K_D represents avidity instead of affinity due to possible bivalent binding of dimeric BMP9 to mAb BMP9-0093.

on pericyte biology. A wound closure assay was used to determine effects of BMP9 on the migration behavior of hPC and HUVEC as a reference. BMP9 treatment (50 ng/ml) did not reduce migration of HUVEC (Figure 4A), while hPC revealed a significant reduction (50%) in migration compared to the control, an effect that was abrogated by treatment with mAb BMP9-0093 (10 µg/ml; Figure 4B, $p = 0.01$). To further investigate the effects of BMP9 on endothelial cell–pericyte interaction *in vitro*, a modified wound healing assay was performed in order to evaluate pericyte attachment to endothelial cells. Stimulation with BMP9 (50 ng/ml) for 48 h caused a reduction in pericyte adherence to HUVEC, whereas pericytes built a monolayer next to endothelial cells in untreated control or mAb BMP9-0093 treated groups (10 µg/ml; Figure 4C). Quantification of red labeled hPC that were located next to green labeled HUVEC confirmed significant inhibition of hPC attachment (Figure 4C; $p = 0.01$). Viability of HUVEC was slightly (10%) increased by BMP9 (50 ng/ml) (Figure S6A, $p < 0.01$ versus control), whereas viability of hPC was slightly (20%) decreased (Figure S6B, $p < 0.001$ versus control). In order to understand the transcriptional changes that are triggered by BMP9 stimulation, we performed RNA sequencing in HUVEC and hPC with and without BMP9 treatment (50 ng/ml; 3 biological replicates per group). Both HUVEC and hPC showed pronounced transcriptional alterations after 8 h of stimulation with BMP9 with 1559 genes being regulated in HUVEC and 441 genes being regulated in hPC (Figure S7). IPA (Ingenuity Pathway Analysis) predicted “angiogenesis” and “cell movement” to be the most significantly affected functions, which is supported by the phenotypic readout in hPC cells that showed reduced cell migration following BMP9 treatment.

3.4. BMP9 signaling is functional in renal carcinoma cells and induces EMT, which can be abrogated by mAb BMP9-0093

A-498 renal cell carcinoma cells lack Endoglin expression, but express several BMP9 receptors like ALK1, ALK2, ALK5, BMPRII, ActRIIA and ActRIIB (Figure 5A). Further, BMP9 treatment (50 ng/ml) induced phosphorylation of Smad 1/5/8 in a time dependent manner which could be abrogated by mAb BMP9-0093 (10 µg/ml; Figure 5B). Smad 2/3 phosphorylation remained unaffected (data not shown). Interestingly, stimulation of A-498 cells with BMP9 (100 ng/ml, 72 h) led to a conversion from epithelial to fibroblastic cell morphology, marked by bigger cells with a spindle-like phenotype in the BMP9-treated group (Figure 5C). Additionally, staining intensity for the

mesenchymal marker Vimentin was also enhanced upon BMP9 stimulation in A-498 cells (Figure 5C). Western blot analysis confirmed upregulation of Vimentin, in addition to an enhanced expression of further EMT markers N-Cadherin, Snail and β -Catenin (Figure 5D). The expression of epithelial markers E-Cadherin and Claudin-1 was downregulated (Figure 5D). The EMT process induced by BMP9 (100 ng/ml) was reversed by mAb BMP9-0093 treatment (10 µg/ml; Figure 5C and D). We were interested if similar EMT inducing effects of BMP9 could also be shown in other renal cell carcinoma cell lines. Western Blot analysis of ACHN, 786-O and Renca cells revealed that appropriate receptors of the TGF β superfamily were expressed in these cell lines and that phosphorylation of Smad 1/5/8 was induced by stimulation with BMP9 (50 ng/ml; Figure S8). Moreover, EMT key transcription factor Snail was upregulated in all RCC cell lines upon BMP9 stimulation (100 ng/ml) for 72 h (Figure S8). Furthermore, we detected enhanced expression of Vimentin in 786-O cells, upregulation of N-Cadherin and downregulation of Claudin-1 in ACHN and 786-O cells and upregulation of β -Catenin in Renca cells, while other markers were not affected (Figure S8). Snail was recently described to mediate resistance to cell death by decreasing Caspase-3 activity (Vega et al., 2004). Based on BMP9-mediated upregulation of Snail, we were interested, whether BMP9 exhibited protective effects on tumor cells. Our data revealed that A-498 cells serum-starved and pre-incubated with BMP9 (100 ng/ml) demonstrated decreased Caspase-3 activity compared to control ($p = 0.01$; Figure 5E). In addition, we studied the effect of BMP9 on the proliferation of A-498 cells *in vitro*, but did not observe a direct proliferative effect of BMP9 (Figure 5F). Stimulation with recombinant ET-1, also released by HUVEC after BMP9 stimulation, however increased proliferation of A-498 cells (Figure 5F and Figure S9).

3.5. Neutralization of BMP9 inhibits growth of A-498 xenografts and mediates an increased mural cell coverage of tumor vessels

The *in vivo* efficacy of mAb BMP9-0093 given once weekly by i.p. injection was tested in established s.c. A-498 xenograft tumors. Anti-BMP9 treatment (10 mg/kg and 25 mg/kg) delayed tumor growth compared to the control group by ~40% (Figure 6A, $n = 10$ mice per group), and to a similar extend as anti-VEGF therapy (data not shown), demonstrating the therapeutic potential of this antibody. Statistically significant differences between control and mAb BMP9-0093 treatment

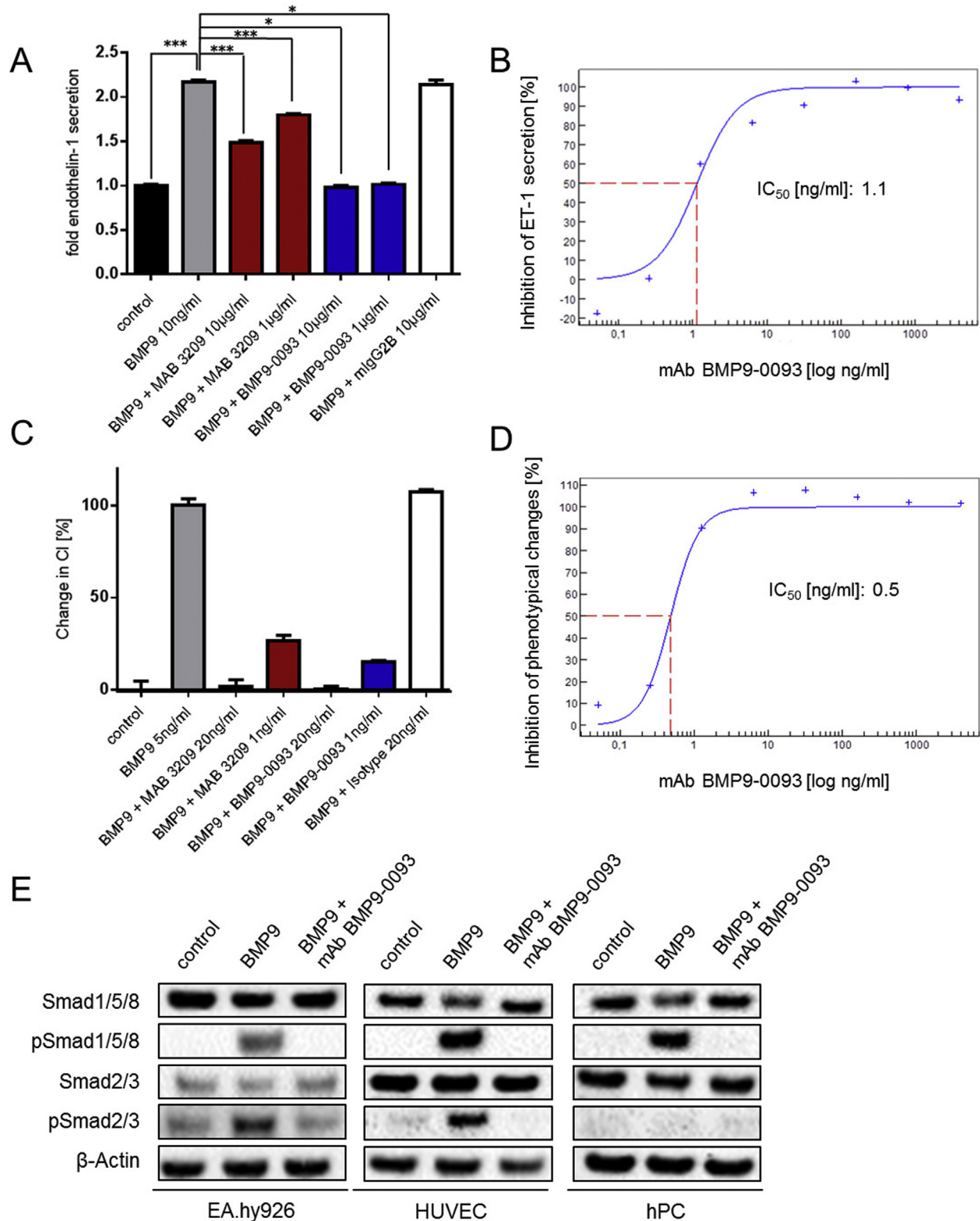


Figure 3 – Modulation of endothelial and pericyte functions and signaling by mAb BMP9-0093. (A) Example for endothelin-1 ELISA functional assay setup using anti-BMP9 mAbs MAB3209 and BMP9-0093 (**p* < 0.05; ****p* < 0.001). (B) Anti-BMP9 mAb BMP9-0093 dose-dependently inhibits BMP9-induced endothelin-1 production by EA.hy926 cells (IC₅₀ = 1.1 ng/ml). (C) Example for functional electronic cell sensor assay (xCELLigence) setup using anti-BMP9 mAbs MAB3209 and BMP9-0093. Cellular phenotypical changes, e.g. attachment and spreading, were recorded in real time and reported as an arbitrary unit (cellular index; CI). (D) Anti-BMP9 mAb BMP9-0093 dose-dependently inhibits BMP9-induced attachment and spreading of EA.hy926 cells (IC₅₀ = 0.5 ng/ml). (E) Western blot analysis of Smad 1/5/8 and Smad 2/3 phosphorylation in EA.hy926, HUVEC and hPC after stimulation with recombinant human BMP9 (50 ng/ml) or a pre-incubated mixture of recombinant human BMP9 (50 ng/ml) and mAb BMP9-0093 (10 μg/ml).

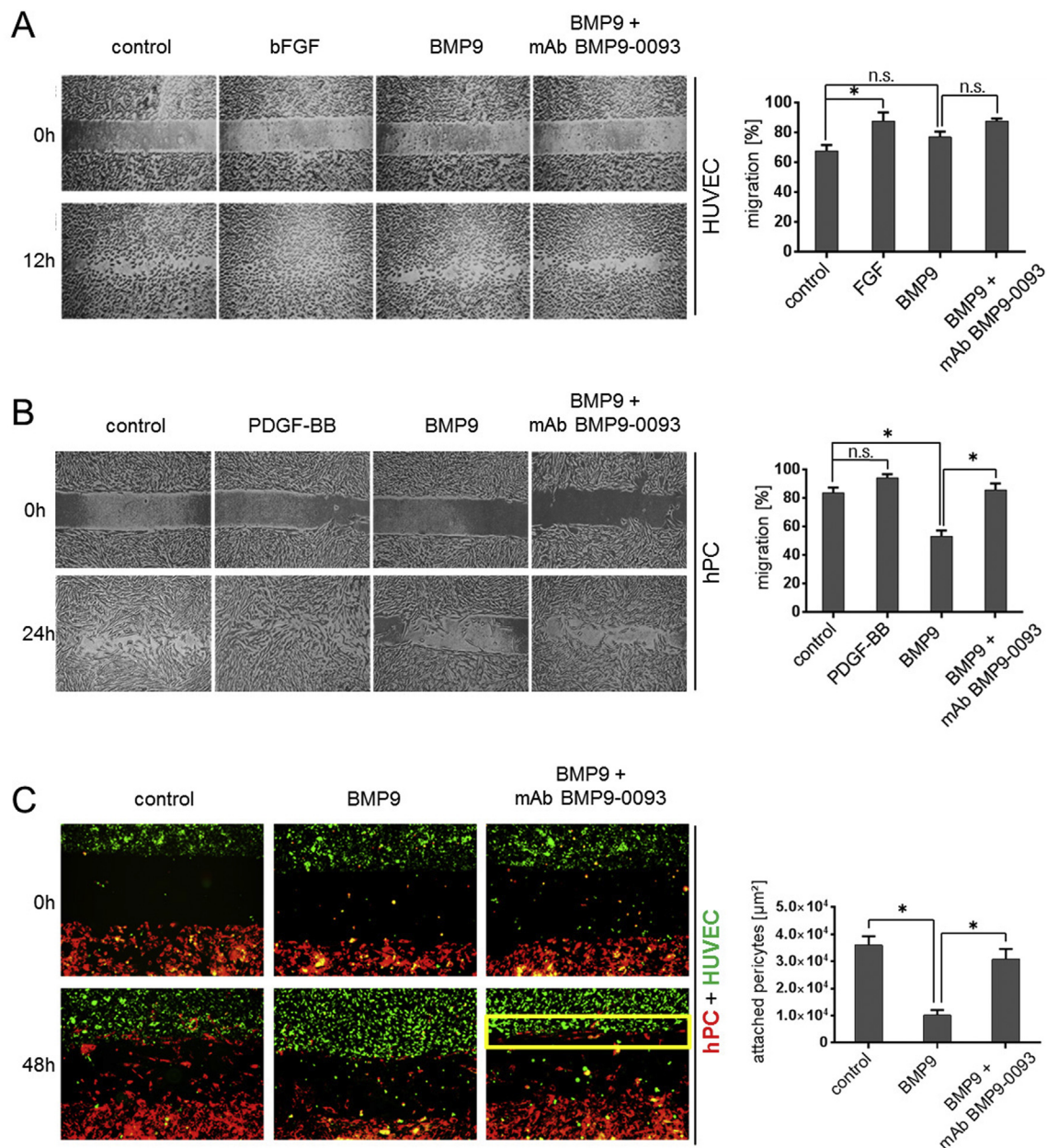


Figure 4 – Anti-BMP9 mAb BMP9-003 restores BMP9-induced decrease in pericyte migration capacity. (A) Quantification and representative pictures of HUVEC migration analyzed at baseline (0 h) and after 12 h. HUVEC were stimulated with dilution buffer (control), bFGF (30 ng/ml), BMP9 (50 ng/ml) or a pre-incubated mixture of BMP9 (50 ng/ml) and mAb BMP9-0093 (10 $\mu\text{g}/\text{ml}$) ($n = 5$). (B) Quantification and representative pictures of hPC migration analyzed at baseline (0 h) and after 24 h. hPC were stimulated with dilution buffer (control), PDGF-BB (40 ng/ml), BMP9 (50 ng/ml) or a pre-incubated mixture of BMP9 (50 ng/ml) and mAb BMP9-0093 (10 $\mu\text{g}/\text{ml}$) ($n = 5$, * $p = 0.01$ versus control). (C) Quantification and representative pictures of hPC (red) attachment to HUVEC (green) at baseline (0 h) and after 48 h. Yellow box marks area used for quantification of red fluorescent hPC. Cells were stimulated with dilution buffer (control), BMP9 (50 ng/ml) or a pre-incubated mixture of BMP9 (50 ng/ml) and mAb BMP9-0093 (10 $\mu\text{g}/\text{ml}$) ($n = 5$, * $p = 0.01$ versus control).

were detected throughout the entire study period (day 28–52; Figure 6A; * $p < 0.05$, ** $p < 0.001$, *** $p < 0.001$). Hemorrhages, often observed in different organs in HHT patients, were not observed during mAb BMP9-0093 *in vivo* treatment (data not shown). In order to elucidate the mechanism of action behind the antitumor efficacy of BMP9 therapy, tumor were excised and analyzed by immunohistochemistry. Tumor cells positive

for phospho-histone H3, a marker for proliferating cells, were significantly decreased in tumors treated with mAb BMP9-0093 compared to vehicle (Figure 6B, $p = 0.02$). Additionally, the apoptosis marker cleaved Caspase-3 was significantly increased after treatment with mAb BMP9-0093 as compared to the control (Figure 6C, $p = 0.01$), indicative for a direct anti-tumor cell effect of anti-BMP9 therapy. Interestingly, we

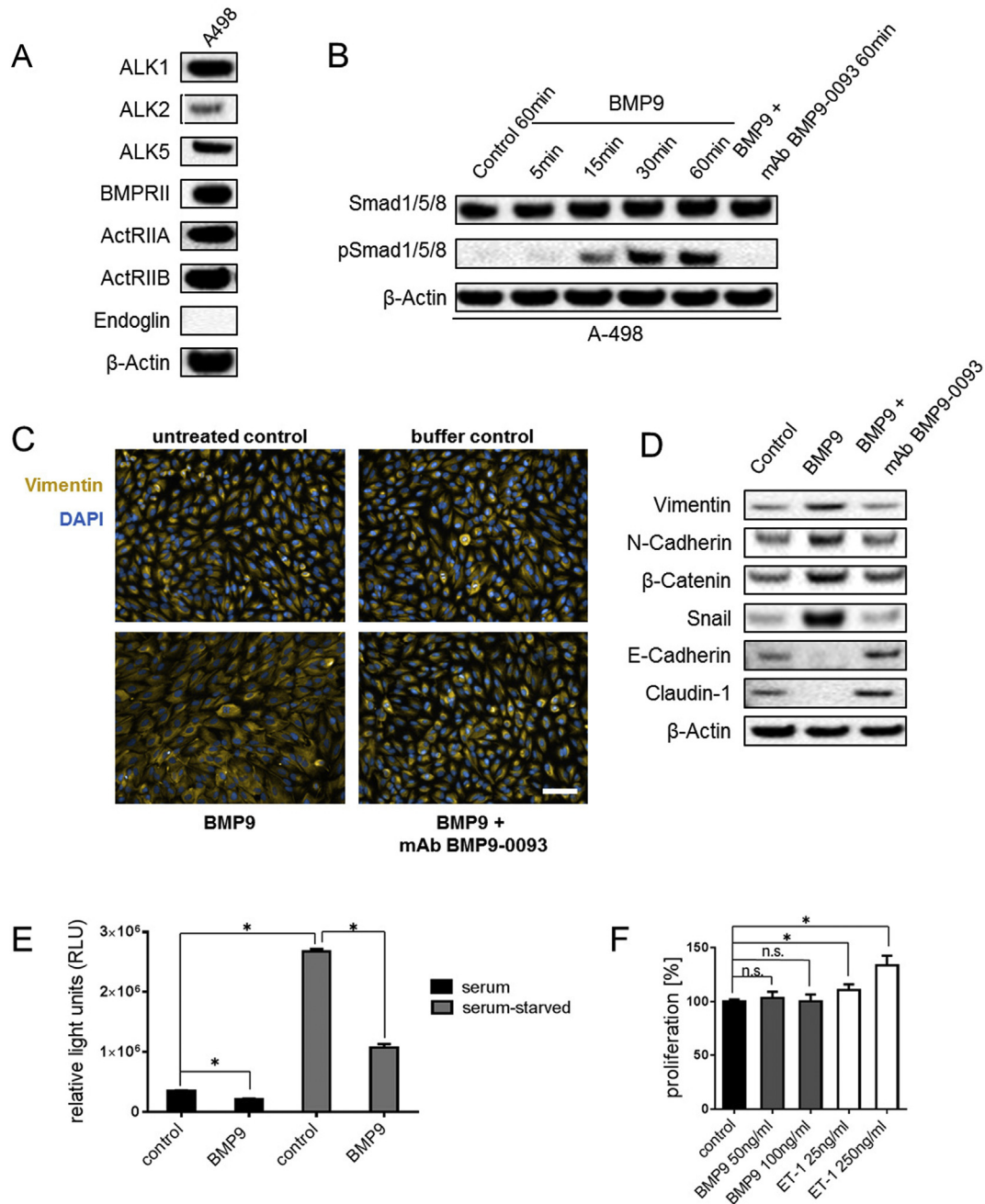


Figure 5 – Anti-BMP9 mAb BMP9-003 interferes with BMP9-mediated Smad phosphorylation and EMT induction. A-498 cells were analyzed by Western blot for (A) expression of BMP9 receptors ALK1, ALK2, BMPRII, ActRIIA, ActRIIB and Endoglin and (B) time dependent phosphorylation of Smad 1/5/8 after BMP9 (50 ng/ml) stimulation and its inhibition by mAb BMP9-0093 (10 µg/ml). (C) Representative images of A-498 cells by PE-Operetta, 20× LD, stained with anti-Vimentin A555 and Hoechst 33258 show increased Vimentin expression and morphologic changes after BMP9 stimulation (100 ng/ml) for 72 h. Scale bars: 100 µm. (D) Regulation of EMT-markers Vimentin, E-Cadherin, N-Cadherin, Claudin-1, β-Catenin and Snail after stimulation with BMP9 (100 ng/ml) for 72 h can be abrogated by treatment with mAb BMP9-0093 (10 µg/ml). (E) Caspase-3 and -7 activity determined by Caspase-Glo[®] 3/7 assay. A-498 were stimulated with BMP9 (100 ng/ml) or medium (control) for 48 h prior to serum starvation for additional 16 h (n = 10; *p = 0.01). (F) Cell viability, indicative for cellular proliferation, determined by CellTiter Glo[®] assay. Results indicate ATP levels normalized to control (n = 10). A-498 cells were treated with dilution buffer (control), BMP9 (50 ng/ml or 100 ng/ml), or ET-1 (25 ng/ml or 250 ng/ml). ET-1 stimulation resulted in significant increase in proliferation (10.7% and 33.7%; p < 0.05 versus control).

detected significant lower levels of ET-1 in tumor lysates of tumors treated with mAb BMP9-0093 compared to control tumors (Figure 6D). Staining of Snail positive nuclei on A-498 tumor slides showed a small but not significant trend towards

a decrease in the anti-BMP9 treatment group (Figure S10). Also vimentin and E-Cadherin were stained on A-498 tumor slides, but no differences were detectable with Vimentin being high expressed and E-Cadherin not detectable on A-498 tumors

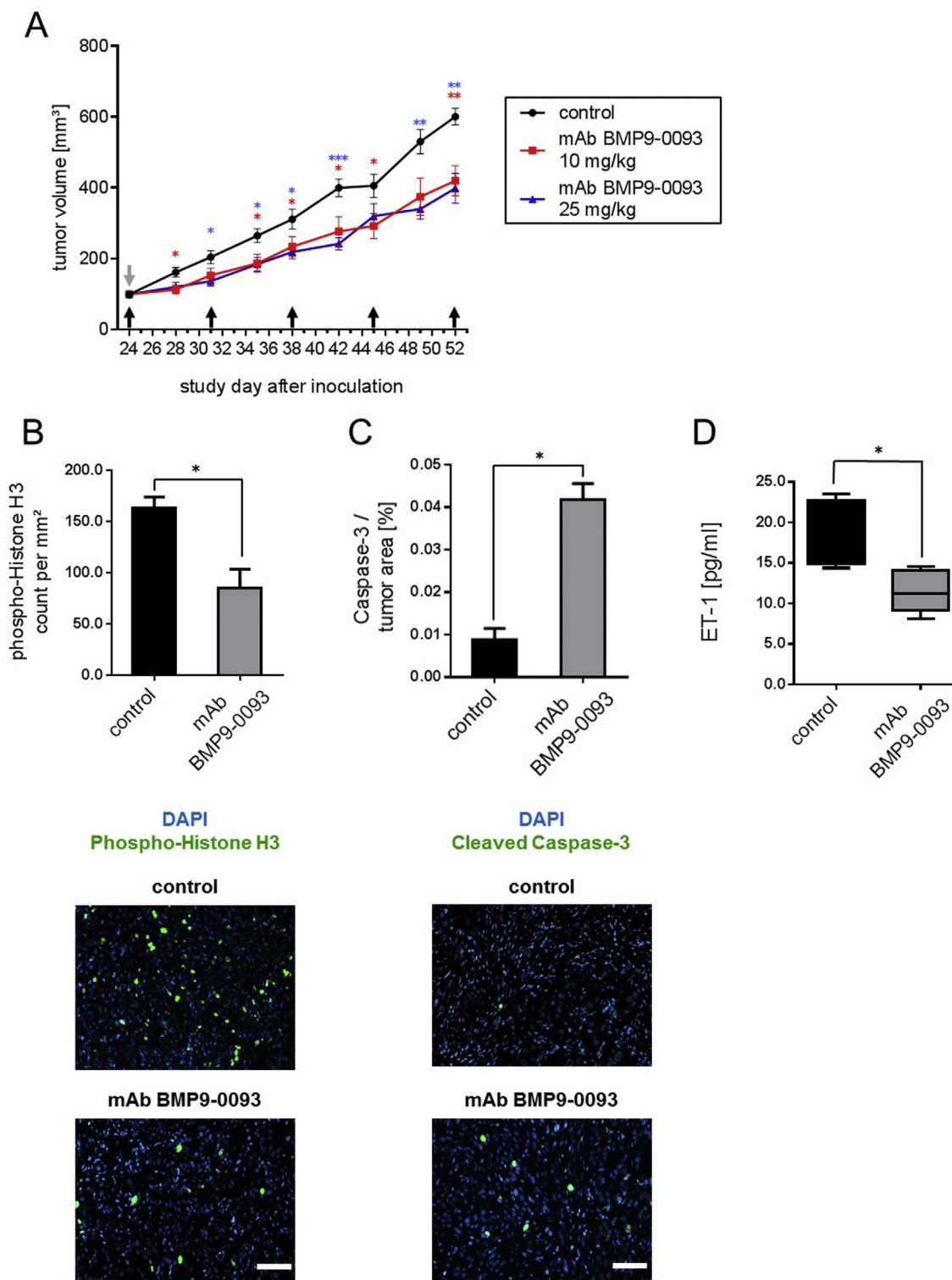


Figure 6 – Anti-BMP9 mAb retards tumor growth of A-498 xenografts. (A) A-498 tumor growth curves in SCID/beige mice receiving anti-BMP9 antibody (mAb BMP9-0093, 10 mg/kg and 25 mg/kg) once weekly (black arrows) i.p. ($n = 10$ mice per group; $*p < 0.05$, $**p < 0.001$, $***p < 0.001$ versus control). Treatment started at day of randomization (grey arrow, day 24). (B) Representative pictures and automated quantification of phospho-histone H3 positive cells per mm² on whole tumor slides ($n = 5$; $p = 0.02$ versus control). Scale bars: 100 μ m. (C) Representative pictures and automated quantification of cleaved Caspase-3 positive area per tumor area on whole tumor slides ($n = 5$; $p = 0.01$ versus control). Scale bars: 100 μ m. (D) Quantification of ET-1 expression in tumor lysates ($n = 5$; $p < 0.05$ versus control). Tumors were collected 7 days after last dosing.

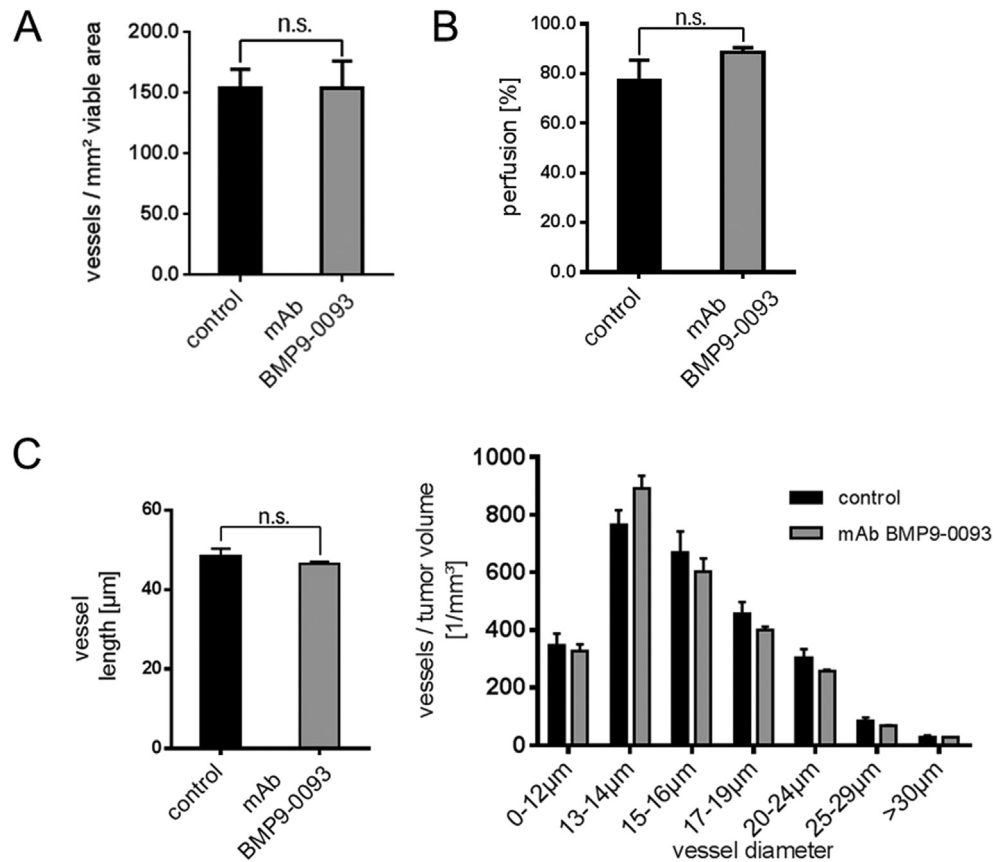


Figure 7 – Neutralization of BMP9 does not affect vascular parameters. (A) Quantitative automated data analysis of CD31⁺ tumor microvessel density on whole tumor slides (MVD; n = 5). (B) Perfusion was assessed based on analysis of lectin-Alexa 750 perfusion and CD31-positive staining in five random regions of 2000 × 1000 µm per tumor slide (n = 5). (C) Quantification of average vascular segment length (left) and distribution of vascular segment diameter (right; n = 5).

(data not shown). Finally, we investigated the impact of treatment with mAb BMP9-0093 on angiogenic activity and maturation of tumor vessels. Although ALK1 was expressed on A-498 tumor endothelial cells (Figure S11), BMP9 blockade had no significant effect on microvascular density and perfusion of tumor vessels (Figure 7A and B; Figure S12). Analysis of tumor vessel architecture by intravenous injection of lectin-Alexa 750 into tumor bearing mice and subsequent ultramicroscopic imaging (Dobosz et al., 2014) also revealed no significant differences in vessel length and diameter between vehicle and mAb BMP9-0093 treated groups (Figure 7C). Notably, we detected increased numbers of NG2 positive cells attached to tumor vessels (Figure 8A, $p = 0.01$). Numbers of α SMA positive cells were only slightly but not significantly increased of, while the numbers of desmin positive cells remained unchanged (Figure 8A). Next, we studied the effect of anti-BMP9 treatment on vascular permeability. Using Alexa 647-labeled omalizumab we found that vascular leakage was decreased in mAb BMP9-0093 treated animals (Figure 8B). This was confirmed by the penetration profile generated by automated quantification of fluorescent signal (Figure 8C). Quantification of the total amount of extravasated labeled antibody demonstrated a significant decrease after mAb

BMP9-0093 treatment compared to control (Figure 8D, $p = 0.04$).

4. Discussion

Although there have been insights into the role of BMP9 signaling in angiogenesis and cancer, the angiogenic and tumor promoting activities of BMP9 remain ambiguous and controversial.

In order to better understand the complex mechanisms underlying BMP9 biology in cancer, we characterized BMP9 expression in the plasma of cancer patients. We found significantly elevated levels of precursor BMP9, suggesting that more BMP9 is produced in cancer patients. We also detected high and significantly increased amounts of pro-domains, with RCC giving a particularly strong response. Reduced levels of mature BMP9 argue for a rapid turnover and internalization of the cytokine, while pro-domains can be considered as left-over of the BMP9•pro-domain complex due to pro-domain displacement after BMP9 receptor binding (Kienast et al., 2016). Supportive of this finding, previous studies showed that the expression of furin, responsible for converting

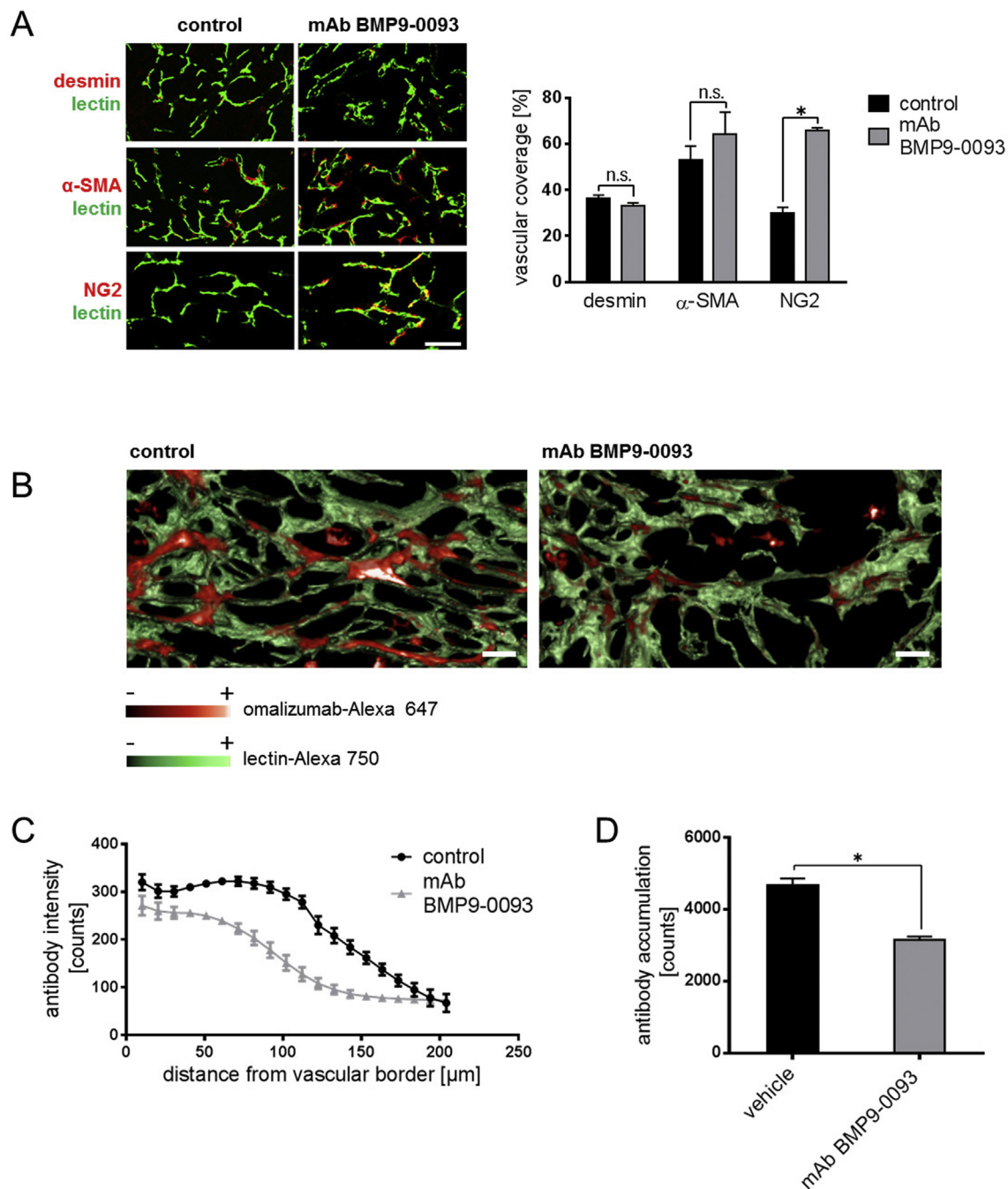


Figure 8 – Inhibition of A-498 tumor growth by BMP9 neutralization is associated with an increase in NG2 positive cell coverage of tumor vessels and reduced penetration of omalizumab-Alexa 647 into tumor tissue. (A) Representative images of IF stained tumor sections and quantification of vessel coverage calculated as the percentage of desmin, α -SMA or NG2 positive vessels in relation to lectin-perfused endothelial cells in five random regions of $2000 \times 1000 \mu\text{m}$ per tumor slide. Anti-BMP9 mAb BMP9-0093 treated tumors showed increased vessel coverage by NG2 positive perivascular cells ($n = 5$ mice per group, $*p = 0.01$ versus control). Scale bars: $100 \mu\text{m}$. Tumors were collected 7 days after last dosing. (B) Representative antibody penetration maps after intravenous injection of omalizumab-Alexa 647 and lectin-Alexa 750. Scale bars: $100 \mu\text{m}$. (C) Penetration profile of omalizumab-Alexa 647 from tumor vessel border to surrounding A-498 tumor tissue ($n = 5$). (D) Total amount of antibody signal calculated as area under the curve of the penetration profile ($n = 5$, $*p = 0.03$ versus control).

precursor BMP9 into the active BMP9•pro-domain variant, is elevated in tumors (Cheng et al., 1997; Khatib et al., 2001; Bassi et al., 2001), suggesting a rapid activation of inactive precursor BMP9 in tumor tissue.

Elevated levels of BMP9 in cancer patients, specifically in RCC, prompted us to evaluate the potential of anti-BMP9 cancer therapy. We generated a BMP9-selective monoclonal antibody, anti-BMP9 mAb BMP9-0093, that targets all of the

different BMP9 variants (BMP9 precursor protein, pro-domain complexed BMP9, and the mature BMP9 cytokine) but does not bind to BMP10. The neutralizing potency of anti-BMP9 mAb BMP9-0093 was demonstrated in multiple biochemical and cellular *in vitro* assays. Furthermore, treatment with mAb BMP9-0093 significantly reduced tumor growth (40%) of A-498 RCC xenografts.

To our surprise, selective BMP9 neutralization had no effect on endothelial cells *in vivo*. We detected no significant decrease in microvascular density (MVD), and further investigations revealed that the vascular architecture remained unaffected by treatment with mAb BMP9-0093 with no effects on vessel length and diameter as well as on vessel perfusion. In contrast, dual neutralization of BMP9/BMP10 by ALK1-Fc (Cunha et al., 2010; Hawinkels et al., 2016; Wang et al., 2016) or ALK1-targeting by a monoclonal antibody (Hu-Lowe et al., 2011) led to tumor growth inhibition associated with a reduction in MVD in several xenograft models. Given the strong angiogenic link for ALK1 signaling in developmental angiogenesis (Johnson et al., 1996), further studies are needed to determine if our results argue for a compensation of BMP9 by BMP10 during tumor angiogenesis, as observed during embryonic vascular development (Ricard et al., 2012; Levet et al., 2013), or if selective BMP9 inhibition simply has no effect on endothelial cells *in vivo*.

Further analyses revealed that the tumor vessels present in the mAb BMP9-0093 treated tumors exhibited increased numbers of NG2 positive pericytes, while these cells were absent or loosely associated with the endothelial cells in the control group. Interestingly, we detected no change in the number of desmin positive cells and only a slight but insignificant change in the number of α -SMA positive cells associated with vascular endothelial cells in mAb BMP9-0093 treated mice. Noteworthy, the observed change in NG2 positive vessel coverage was accompanied by a reduction in vessel leakiness, arguing for a functional role of NG2 positive cells in vascular permeability and possibly maturation. A decrease in vessel leakiness may counteract the development of metastasis (Kienast et al., 2013). Unfortunately, the tumor model used here only rarely results in spontaneous metastases. A recently published study on ALK1-Fc in breast cancer however indeed showed an effect on metastasis formation and defines endothelial expression of ALK1 as an independent and highly specific prognostic factor for metastatic manifestation (Cunha et al., 2015). EMT is an important mechanism related to cancer invasion and metastasis (Yang and Weinberg, 2008). Interestingly, we detected BMP9-mediated induction of EMT *in vitro*, previously also shown in HCC cells (Li et al., 2013). We however observed only a small but not significant trend towards a decrease in Snail expression in mAb BMP9-0093 treated A-498 tumors, underscoring the complexity of EMT and raising the question, if prevention of EMT *in vitro* may be more effective than blockade of EMT that has already taken place *in vivo*. Therefore, the role of BMP9 in EMT and metastasis warrants further investigation.

Our present study corroborated the data obtained in previous studies, in which dual BMP9/BMP10 inhibition could also increase pericyte coverage of tumor vessels (Cunha et al., 2010; Hawinkels et al., 2016) and is in line with our *in vitro* data, demonstrating a BMP9-induced decrease in pericyte

migration and attachment to endothelial cells that could be reversed by mAb BMP9-0093 treatment. Interestingly, this data adds to the growing body of evidence for a pleiotropic role of BMP9 in development and disease. While a defective paracrine signaling between endothelial cells and the neighboring mural cells may be one of the underlying causes of HHT (Thalgott et al., 2015), neutralization of BMP9 in tumor angiogenesis may lead to opposing effects, as indicated by increased numbers of pericyte covered tumor vessels.

To the best of our knowledge, we are the first to report a direct effect of BMP9 on pericyte signaling and migration *in vitro*. Here, we detected Smad 1/5/8 phosphorylation in pericytes in response to BMP9, while in endothelial cells BMP-9 was capable of inducing both Smad 1/5/8 and Smad 2/3 phosphorylation, which is in line with previous findings (Upton et al., 2009). The difference in Smad phosphorylation observed is intriguing, as the expression pattern of all type I and II receptors is similar between endothelial cells and pericytes, except for ALK2, which can be detected on pericytes, but not on endothelial cells. RNAseq analysis demonstrated that endothelial cells and pericytes were differentially regulated by BMP9. In addition, we found that migration behavior of pericytes but not HUVEC was influenced by BMP9. Further investigations are necessary to understand the significance of this difference in phosphorylation pattern in endothelial cells and pericytes.

While the functions of TGF β in carcinogenesis and tumor progression have been intensely studied, the function of BMP9 in cancer biology remains less understood (Wakefield and Hill, 2013). TGF β serves as a tumor suppressor in pre-malignant cells, whereas it functions as a tumor promoter in later stages of cancer development. Bone morphogenic proteins BMP4 and BMP7 were shown to participate in tumor progression (Guo et al., 2012; Lu et al., 2012), whereas BMP2 was shown to function in both pro- or anti-tumorigenic roles (Wen et al., 2004; Qiu et al., 2010), similar to BMP9. In this way, BMP9 was shown to provide tumor suppressor activity in prostate (Ye et al., 2008) and breast cancer (Wang et al., 2011), but tumor promoting activity in HCC (Li et al., 2013) and ovarian cancer (Herrera et al., 2009), while its role in RCC remained unclear. Our own data revealed a direct effect of BMP9 on A-498 and other RCC tumor cells, demonstrated by time dependent phosphorylation of Smad 1/5/8. These results were supplemented by a tumor cell protective effect of BMP9 *in vitro* as well as an anti-proliferative and pro-apoptotic effect of BMP9 targeted therapy *in vivo*. Interestingly, we detected significant lower levels of ET-1 *ex vivo* in tumor lysates of tumors treated with mAb BMP9-0093 compared to control tumors. This may be a first hint that the effect on proliferation of A-498 tumor cells *in vivo* can be indirectly influenced by BMP9 through other cells of the tumor stroma, e.g. endothelial cells of the tumor vasculature.

Taken together, our findings implicate the BMP9/Smad pathway as a potential promoter of tumor growth. Selective anti-BMP9 treatment retards tumor growth *in vivo* and affects tumor vessel associated perivascular cell attachment. The concept of anti-angiogenic therapy has evolved from starving tumors to normalization of tumor vasculature (Jain, 2014). An increased vascular coverage and reduced vessel leakiness, but lack of major vessel deprivation as observed with selective

anti-BMP9 therapy in this study, is in support of this hypothesis.

Financial disclosure

The authors are employees of Roche Diagnostics GmbH.

Acknowledgements

We would like to acknowledge the valuable technical support provided by (in alphabetical order) Juliane Braun, Ulrike Ebert, Gerlind Herberich, Gabriele Jobs, Franziska Mech, Sabine Schuster, Petra Ulrich, Renko Wenig, Guido Werner, and Florian Zitzelsberger. We thank Dr. Markus Thomas, Dr. Stefan Ries and Dr. Rainer Constien for strategic advice and scientific support. This present work was performed in fulfillment of the requirements for obtaining the degree “Dr. rer. nat.” of Verena Brand.

Appendix A. Supplementary data

Supplementary data related to this article can be found at <http://dx.doi.org/10.1016/j.molonc.2016.10.002>.

REFERENCES

- Bassi, D.E., Mahloogi, H., Al-Saleem, L., Lopez De, C.R., Ridge, J.A., Klein-Szanto, A.J., 2001. Elevated furin expression in aggressive human head and neck tumors and tumor cell lines. *Mol. Carcinog.* 31, 224–232.
- Beger, B., Robertson, K., Evans, A., Grant, A., Berg, J., 2006. Expression of endoglin and the activin receptor-like kinase 1 in skin suggests a role for these receptors in normal skin function and skin tumorigenesis. *Br. J. Dermatol.* 154, 379–382.
- Bidart, M., Ricard, N., Levet, S., Samson, M., Mallet, C., David, L., Subileau, M., Tillet, E., Feige, J.J., Bailly, S., 2012. BMP9 is produced by hepatocytes and circulates mainly in an active mature form complexed to its prodomain. *Cell Mol. Life Sci.* 69, 313–324.
- Bourdeau, A., Faughnan, M.E., Letarte, M., 2000. Endoglin-deficient mice, a unique model to study hereditary hemorrhagic telangiectasia. *Trends Cardiovasc. Med.* 10, 279–285.
- Brown, M.A., Zhao, Q., Baker, K.A., Naik, C., Chen, C., Pukac, L., Singh, M., Tsareva, T., Parice, Y., Mahoney, A., Roschke, V., Sanyal, I., Choe, S., 2005. Crystal structure of BMP-9 and functional interactions with pro-region and receptors. *J. Biol. Chem.* 280, 25111–25118.
- Chen, C., Grzegorzewski, K.J., Barash, S., Zhao, Q., Schneider, H., Wang, Q., Singh, M., Pukac, L., Bell, A.C., Duan, R., Coleman, T., Duttaroy, A., Cheng, S., Hirsch, J., Zhang, L., Lazard, Y., Fischer, C., Barber, M.C., Ma, Z.D., Zhang, Y.Q., Reavey, P., Zhong, L., Teng, B., Sanyal, I., Ruben, S.M., Blondel, O., Birse, C.E., 2003. An integrated functional genomics screening program reveals a role for BMP-9 in glucose homeostasis. *Nat. Biotechnol.* 21, 294–301.
- Chen, H., Brady, R.J., Sai, T., Lai, J., Warming, S., Chen, H., Rose-Girma, M., Zhang, G., Shou, W., Yan, M., 2013. Context-dependent signaling defines roles of BMP9 and BMP10 in embryonic and postnatal development. *Proc. Natl. Acad. Sci. U. S. A.* 110, 11887–11892.
- Cheng, M., Watson, P.H., Paterson, J.A., Seidah, N., Chretien, M., Shiu, R.P., 1997. Pro-protein convertase gene expression in human breast cancer. *Int. J. Cancer* 71, 966–971.
- Cunha, S.I., Bocci, M., Lovrot, J., Eleftheriou, N., Roswall, P., Cordero, E., Lindstrom, L., Bartoschek, M., Haller, B.K., Pearsall, R.S., Mulivor, A.W., Kumar, R., Larsson, C., Bergh, J., Pietras, K., 2015. Endothelial ALK1 is a therapeutic target to block metastatic dissemination of breast cancer. *Cancer Res.* 75, 2445–2456.
- Cunha, S.I., Pardali, E., Thorikay, M., Anderberg, C., Hawinkels, L., Goumans, M.J., Seehra, J., Heldin, C.H., ten Dijke, P., Pietras, K., 2010. Genetic and pharmacological targeting of activin receptor-like kinase 1 impairs tumor growth and angiogenesis. *J. Exp. Med.* 207, 85–100.
- Cunha, S.I., Pietras, K., 2011. ALK1 as an emerging target for antiangiogenic therapy of cancer. *Blood* 117, 6999–7006.
- David, L., Mallet, C., Keramidis, M., Lamande, N., Gasc, J.M., Dupuis-Girod, S., Plauchu, H., Feige, J.J., Bailly, S., 2008. Bone morphogenetic protein-9 is a circulating vascular quiescence factor. *Circ. Res.* 102, 914–922.
- David, L., Mallet, C., Mazerbourg, S., Feige, J.J., Bailly, S., 2007. Identification of BMP9 and BMP10 as functional activators of the orphan activin receptor-like kinase 1 (ALK1) in endothelial cells. *Blood* 109, 1953–1961.
- Dobosz, M., Ntziachristos, V., Scheuer, W., Strobel, S., 2014. Multispectral fluorescence ultramicroscopy: three-dimensional visualization and automatic quantification of tumor morphology, drug penetration, and antiangiogenic treatment response. *Neoplasia* 16, 1–13.
- Dotz, H.U., Leischner, U., Schierloh, A., Jahrling, N., Mauch, C.P., Deininger, K., Deussing, J.M., Eder, M., Ziegler, W., Becker, K., 2007. Ultramicroscopy: three-dimensional visualization of neuronal networks in the whole mouse brain. *Nat. Methods* 4, 331–336.
- Duarte, C.W., Murray, K., Lucas, F.L., Fairfield, K., Miller, H., Brooks, P., Vary, C.P., 2014. Improved survival outcomes in cancer patients with hereditary hemorrhagic telangiectasia. *Cancer Epidemiol. Biomark. Prev.* 23, 117–125.
- Edgell, C.J., Haizlip, J.E., Bagnell, C.R., Packenham, J.P., Harrison, P., Wilbourn, B., Madden, V.J., 1990. Endothelium specific Weibel-Palade bodies in a continuous human cell line, EA.hy926. *In Vitro Cell Dev. Biol.* 26, 1167–1172.
- Edgell, C.J., McDonald, C.C., Graham, J.B., 1983. Permanent cell line expressing human factor VIII-related antigen established by hybridization. *Proc. Natl. Acad. Sci. U. S. A.* 80, 3734–3737.
- Finsson, K.W., Parker, W.L., ten, D.P., Thorikay, M., Philip, A., 2008. ALK1 opposes ALK5/Smad3 signaling and expression of extracellular matrix components in human chondrocytes. *J. Bone Miner. Res.* 23, 896–906.
- Guo, X., Xiong, L., Zou, L., Zhao, J., 2012. Upregulation of bone morphogenetic protein 4 is associated with poor prognosis in patients with hepatocellular carcinoma. *Pathol. Oncol. Res.* 18, 635–640.
- Hawinkels, L.J., de Vinuesa, A.G., Paauwe, M., Kruihof-de, J.M., Wiercinska, E., Pardali, E., Mezzanotte, L., Keereweer, S., Braumuller, T.M., Heijkants, R.C., Jonkers, J., Lowik, C.W., Goumans, M.J., Ten Hagen, T.L., ten, D.P., 2016. Activin receptor-like kinase 1 ligand trap reduces microvascular density and improves chemotherapy efficiency to various solid tumors. *Clin. Cancer Res.* 22, 96–106.
- Herrera, B., Dooley, S., Breitkopf-Heinlein, K., 2014. Potential roles of bone morphogenetic protein (BMP)-9 in human liver diseases. *Int. J. Mol. Sci.* 15, 5199–5220.
- Herrera, B., Garcia-Alvaro, M., Cruz, S., Walsh, P., Fernandez, M., Roncero, C., Fabregat, I., Sanchez, A., Inman, G.J., 2013. BMP9 is

- a proliferative and survival factor for human hepatocellular carcinoma cells. *PLoS One* 8, e69535.
- Herrera, B., van, D.M., ten, D.P., Inman, G.J., 2009. Autocrine bone morphogenetic protein-9 signals through activin receptor-like kinase-2/Smad1/Smad4 to promote ovarian cancer cell proliferation. *Cancer Res.* 69, 9254–9262.
- Hu-Lowe, D.D., Chen, E., Zhang, L., Watson, K.D., Mancuso, P., Lappin, P., Wickman, G., Chen, J.H., Wang, J., Jiang, X., Amundson, K., Simon, R., Erbersdobler, A., Bergqvist, S., Feng, Z., Swanson, T.A., Simmons, B.H., Lippincott, J., Caspersen, G.F., Levin, W.J., Stampino, C.G., Shalinsky, D.R., Ferrara, K.W., Fiedler, W., Bertolini, F., 2011. Targeting activin receptor-like kinase 1 inhibits angiogenesis and tumorigenesis through a mechanism of action complementary to anti-VEGF therapies. *Cancer Res.* 71, 1362–1373.
- Jain, R.K., 2014. Antiangiogenesis strategies revisited: from starving tumors to alleviating hypoxia. *Cancer Cell* 26, 605–622.
- Johnson, D.W., Berg, J.N., Baldwin, M.A., Gallione, C.J., Marondel, I., Yoon, S.J., Stenzel, T.T., Speer, M., Pericak-Vance, M.A., Diamond, A., Guttmacher, A.E., Jackson, C.E., Attisano, L., Kucherlapati, R., Porteous, M.E., Marchuk, D.A., 1996. Mutations in the activin receptor-like kinase 1 gene in hereditary haemorrhagic telangiectasia type 2. *Nat. Genet.* 13, 189–195.
- Khatib, A.M., Siegfried, G., Prat, A., Luis, J., Chretien, M., Metrakos, P., Seidah, N.G., 2001. Inhibition of proprotein convertases is associated with loss of growth and tumorigenicity of HT-29 human colon carcinoma cells: importance of insulin-like growth factor-1 (IGF-1) receptor processing in IGF-1-mediated functions. *J. Biol. Chem.* 276, 30686–30693.
- Kienast, Y., Jucknischke, U., Scheiblich, S., Thier, M., de, W.M., Haas, A., Lehmann, C., Brand, V., Bernicke, D., Honold, K., Lorenz, S., 2016. Rapid activation of bone morphogenetic protein 9 by receptor-mediated displacement of pro-domains. *J. Biol. Chem.* 291, 3395–3410.
- Kienast, Y., Klein, C., Scheuer, W., Raemsch, R., Lorenzon, E., Bernicke, D., Herting, F., Yu, S., The, H.H., Martarello, L., Gassner, C., Stubenrauch, K.G., Munro, K., Augustin, H.G., Thomas, M., 2013. Ang-2-VEGF-A CrossMab, a novel bispecific human IgG1 antibody blocking VEGF-a and Ang-2 functions simultaneously, mediates potent antitumor, antiangiogenic, and antimetastatic efficacy. *Clin. Cancer Res.* 19, 6730–6740.
- König, H.G., Kogel, D., Rami, A., Prehn, J.H., 2005. TGF- β 1 activates two distinct type I receptors in neurons: implications for neuronal NF- κ B signaling. *J. Cell Biol.* 168, 1077–1086.
- Lamouille, S., Mallet, C., Feige, J.J., Bailly, S., 2002. Activin receptor-like kinase 1 is implicated in the maturation phase of angiogenesis. *Blood* 100, 4495–4501.
- Larrievé, B., Prahst, C., Gordon, E., del, T.R., Mathivet, T., Duarte, A., Simons, M., Eichmann, A., 2012. ALK1 signaling inhibits angiogenesis by cooperating with the Notch pathway. *Dev. Cell* 22, 489–500.
- Levet, S., Ciais, D., Merdzhanova, G., Mallet, C., Zimmers, T.A., Lee, S.J., Navarro, F.P., Texier, I., Feige, J.J., Bailly, S., Vittet, D., 2013. Bone morphogenetic protein 9 (BMP9) controls lymphatic vessel maturation and valve formation. *Blood* 122, 598–607.
- Li, Q., Gu, X., Weng, H., Ghafoory, S., Liu, Y., Feng, T., Dzieran, J., Li, L., Ilkavets, I., Kruihof-de, J.M., Munker, S., Marx, A., Piiper, A., Augusto, A.E., Gretz, N., Gao, C., Wolf, S., Dooley, S., Breitkopf-Heinlein, K., 2013. Bone morphogenetic protein-9 induces epithelial to mesenchymal transition in hepatocellular carcinoma cells. *Cancer Sci.* 104, 398–408.
- Lopez-Coviella, I., Berse, B., Krauss, R., Thies, R.S., Blusztajn, J.K., 2000. Induction and maintenance of the neuronal cholinergic phenotype in the central nervous system by BMP-9. *Science* 289, 313–316.
- Lu, J.W., Hsia, Y., Yang, W.Y., Lin, Y.I., Li, C.C., Tsai, T.F., Chang, K.W., Shieh, G.S., Tsai, S.F., Wang, H.D., Yuh, C.H., 2012. Identification of the common regulators for hepatocellular carcinoma induced by hepatitis B virus X antigen in a mouse model. *Carcinogenesis* 33, 209–219.
- Luther, G., Wagner, E.R., Zhu, G., Kang, Q., Luo, Q., Lamplot, J., Bi, Y., Luo, X., Luo, J., Teven, C., Shi, Q., Kim, S.H., Gao, J.L., Huang, E., Yang, K., Rames, R., Liu, X., Li, M., Hu, N., Liu, H., Su, Y., Chen, L., He, B.C., Zuo, G.W., Deng, Z.L., Reid, R.R., Luu, H.H., Haydon, R.C., He, T.C., 2011. BMP-9 induced osteogenic differentiation of mesenchymal stem cells: molecular mechanism and therapeutic potential. *Curr. Gene Ther.* 11, 229–240.
- Mancini, M.L., Verdi, J.M., Conley, B.A., Nicola, T., Spicer, D.B., Oxburgh, L.H., Vary, C.P., 2007. Endoglin is required for myogenic differentiation potential of neural crest stem cells. *Dev. Biol.* 308, 520–533.
- McAllister, K.A., Grogg, K.M., Johnson, D.W., Gallione, C.J., Baldwin, M.A., Jackson, C.E., Helmbold, E.A., Markel, D.S., McKinnon, W.C., Murrell, J., 1994. Endoglin, a TGF- β binding protein of endothelial cells, is the gene for hereditary haemorrhagic telangiectasia type 1. *Nat. Genet.* 8, 345–351.
- Olsen, O.E., Wader, K.F., Misund, K., Vatsveen, T.K., Ro, T.B., Mylin, A.K., Turesson, I., Stordal, B.F., Moen, S.H., Standal, T., Waage, A., Sundan, A., Holien, T., 2014. Bone morphogenetic protein-9 suppresses growth of myeloma cells by signaling through ALK2 but is inhibited by endoglin. *Blood Cancer J.* 4, e196.
- Pflug, B.R., Zheng, H., Udan, M.S., D'Antonio, J.M., Marshall, F.F., Brooks, J.D., Nelson, J.B., 2007. Endothelin-1 promotes cell survival in renal cell carcinoma through the ET(A) receptor. *Cancer Lett.* 246, 139–148.
- Qiu, H., Yang, B., Pei, Z.C., Zhang, Z., Ding, K., 2010. WSS25 inhibits growth of xenografted hepatocellular cancer cells in nude mice by disrupting angiogenesis via blocking bone morphogenetic protein (BMP)/Smad/Id1 signaling. *J. Biol. Chem.* 285, 32638–32646.
- Ricard, N., Ciais, D., Levet, S., Subileau, M., Mallet, C., Zimmers, T.A., Lee, S.J., Bidart, M., Feige, J.J., Bailly, S., 2012. BMP9 and BMP10 are critical for postnatal retinal vascular remodeling. *Blood* 119, 6162–6171.
- Sanz-Rodríguez, F., Fernández, L., Zarrabeitia, R., Perez-Molino, A., Ramirez, J.R., Coto, E., Bernabeu, C., Botella, L.M., 2004. Mutation analysis in Spanish patients with hereditary hemorrhagic telangiectasia: deficient endoglin up-regulation in activated monocytes. *Clin. Chem.* 50, 2003–2011.
- Scharpfenecker, M., van Dinther, M., Liu, Z., van Bezooijen, R.L., Zhao, Q., Pukac, L., Löwik, C.W.G.M., ten Dijke, P., 2007. BMP-9 signals via ALK1 and inhibits bFGF-induced endothelial cell proliferation and VEGF-stimulated angiogenesis. *J. Cell Sci.* 120, 964–972.
- Srinivasan, S., Hanes, M.A., Dickens, T., Porteous, M.E., Oh, S.P., Hale, L.P., Marchuk, D.A., 2003. A mouse model for hereditary hemorrhagic telangiectasia (HHT) type 2. *Hum. Mol. Genet.* 12, 473–482.
- Star, G.P., Giovinazzo, M., Langleben, D., 2010. Bone morphogenetic protein-9 stimulates endothelin-1 release from human pulmonary microvascular endothelial cells: a potential mechanism for elevated ET-1 levels in pulmonary arterial hypertension. *Microvasc. Res.* 80, 349–354.
- Su, A.I., Wiltshire, T., Batalov, S., Lapp, H., Ching, K.A., Block, D., Zhang, J., Soden, R., Hayakawa, M., Kreiman, G., Cooke, M.P., Walker, J.R., Hogenesch, J.B., 2004. A gene atlas of the mouse and human protein-encoding transcriptomes. *Proc. Natl. Acad. Sci. U. S. A.* 101, 6062–6067.

- Suzuki, Y., Ohga, N., Morishita, Y., Hida, K., Miyazono, K., Watabe, T., 2010. BMP-9 induces proliferation of multiple types of endothelial cells in vitro and in vivo. *J. Cell Sci.* 123, 1684–1692.
- Takahashi, N., Haba, A., Matsuno, F., Seon, B.K., 2001. Antiangiogenic therapy of established tumors in human skin/severe combined immunodeficiency mouse chimeras by anti-endoglin (CD105) monoclonal antibodies, and synergy between anti-endoglin antibody and cyclophosphamide. *Cancer Res.* 61, 7846–7854.
- Thalgott, J., Dos-Santos-Luis, D., Lebrin, F., 2015. Pericytes as targets in hereditary hemorrhagic telangiectasia. *Front Genet.* 6, 37.
- Upton, P.D., Davies, R.J., Trembath, R.C., Morrell, N.W., 2009. Bone morphogenetic protein (BMP) and activin type II receptors balance BMP9 signals mediated by activin receptor-like kinase-1 in human pulmonary artery endothelial cells. *J. Biol. Chem.* 284, 15794–15804.
- Vega, S., Morales, A.V., Ocana, O.H., Valdes, F., Fabregat, I., Nieto, M.A., 2004. Snail blocks the cell cycle and confers resistance to cell death. *Genes Dev.* 18, 1131–1143.
- Velasco, S., varez-Munoz, P., Pericacho, M., Dijke, P.T., Bernabeu, C., Lopez-Novoa, J.M., Rodriguez-Barbero, A., 2008. L- and S-endoglin differentially modulate TGFbeta1 signaling mediated by ALK1 and ALK5 in L6E9 myoblasts. *J. Cell Sci.* 121, 913–919.
- Wakefield, L.M., Hill, C.S., 2013. Beyond TGFbeta: roles of other TGFbeta superfamily members in cancer. *Nat. Rev. Cancer* 13, 328–341.
- Wang, K., Feng, H., Ren, W., Sun, X., Luo, J., Tang, M., Zhou, L., Weng, Y., He, T.C., Zhang, Y., 2011. BMP9 inhibits the proliferation and invasiveness of breast cancer cells MDA-MB-231. *J. Cancer Res. Clin. Oncol.* 137, 1687–1696.
- Wang, X., Solban, N., Khanna, P., Callea, M., Song, J., Alsop, D.C., Pearsall, R.S., Atkins, M.B., Mier, J.W., Signoretti, S., Alimzhanov, M., Kumar, R., Bhasin, M.K., Bhatt, R.S., 2016. Inhibition of ALK1 signaling with dalantercept combined with VEGFR TKI leads to tumor stasis in renal cell carcinoma. *Oncotarget.*
- Wen, X.Z., Miyake, S., Akiyama, Y., Yuasa, Y., 2004. BMP-2 modulates the proliferation and differentiation of normal and cancerous gastric cells. *Biochem. Biophys. Res. Commun.* 316, 100–106.
- Wooderchak-Donahue, W.L., McDonald, J., O'Fallon, B., Upton, P.D., Li, W., Roman, B.L., Young, S., Plant, P., Fulop, G.T., Langa, C., Morrell, N.W., Botella, L.M., Bernabeu, C., Stevenson, D.A., Runo, J.R., Bayrak-Toydemir, P., 2013. BMP9 mutations cause a vascular-anomaly syndrome with phenotypic overlap with hereditary hemorrhagic telangiectasia. *Am. J. Hum. Genet.* 93, 530–537.
- Yang, J., Weinberg, R.A., 2008. Epithelial-mesenchymal transition: at the crossroads of development and tumor metastasis. *Dev. Cell* 14, 818–829.
- Ye, L., Kynaston, H., Jiang, W.G., 2008. Bone morphogenetic protein-9 induces apoptosis in prostate cancer cells, the role of prostate apoptosis response-4. *Mol. Cancer Res.* 6, 1594–1606.
- Yoshimatsu, Y., Lee, Y.G., Akatsu, Y., Taguchi, L., Suzuki, H.I., Cunha, S.I., Maruyama, K., Suzuki, Y., Yamazaki, T., Katsura, A., Oh, S.P., Zimmers, T.A., Lee, S.J., Pietras, K., Koh, G.Y., Miyazono, K., Watabe, T., 2013. Bone morphogenetic protein-9 inhibits lymphatic vessel formation via activin receptor-like kinase 1 during development and cancer progression. *Proc. Natl. Acad. Sci. U. S. A.* 110, 18940–18945.